Ore Geology Reviews 82 (2017) 198–216

Contents lists available at ScienceDirect

Ore Geology Reviews

journal homepage: www.elsevier.com/locate/oregeo

Importance of hydrogeological conditions during formation of the karstic bauxite deposits, Central Guizhou Province, Southwest China: A case study at Lindai deposit

Kun-Yue Ling [a], Xiao-Qing Zhu [a,*], Hao-Shu Tang [a,*], Shi-Xin Li [b]

[a] State Key Laboratory of Ore Deposit Geochemistry, Institute of Geochemistry, Chinese Academy of Sciences, Guiyang 550081, China
[b] Geological Constructing Branch Co., Donghua Construction Co., Yankuang Group, Zoucheng 273500, Shandong, China

ARTICLE INFO

Article history:
Received 1 March 2016
Received in revised form 27 November 2016
Accepted 29 November 2016
Available online 8 December 2016

Keywords:
Simulated weathering experiments
Hydrogeological conditions
"Coal–bauxite–iron" structure
Karstic bauxite metallogenic model

ABSTRACT

Karstic bauxite deposits are widespread in Central Guizhou Province, SW China, and high-grade ores are frequently sandwiched with overlying coal and underlying iron-rich layers and form a special "coal–bauxite–iron" structure. The Lindai deposit, which is one of the most representative karstic bauxite deposits in Central Guizhou Province, was selected as a case study. Based on textural features and iron abundances, bauxite ores in the Lindai deposit are divided into three types of ores, i.e., clastic, compact, and high-iron. The bauxite ores primarily comprise diaspore, boehmite, kaolinite, illite, and hematite with minor quartz, smectite, pyrite, zircon, rutile, anatase, and feldspar. The Al_2O_3 (53–76.8 wt.%) is the main chemical contents of the bauxite ore samples in the Lindai district, followed by SiO_2, Fe_2O_3, TiO_2, CaO, MgO, S, and P etc. Our geological data on the Lindai deposit indicated that the ore-bearing rock series and its underlying stratum have similar rare earth elements distribution pattern and similar Y/Ho, Zr/Hf, and Eu/Eu* values; additionally, all ore-bearing rock samples are rich in MgO (range from 0.16 wt.% to 0.68 wt.%), and the plots of the dolomites and laterites lie almost on or close to the weathering line fit by the Al-bearing rocks in Zr vs. Hf and Nb vs. Ta diagrams; suggesting that the underlying Middle Cambrian Shilengshui Formation dolomite is the parent rock of bauxite resources in the Lindai district.

Simulated weathering experiments on the modern laterite from the Shilengshui Formation dolomite in the Lindai bauxite deposit show that hydrogeological conditions are important for karstic bauxite formation: Si is most likely to migrate, its migration rate is several magnitudes higher than those of Al and Fe under natural conditions; the reducing inorganic acid condition is the most conducive to Al enrichment and Si removal; Fe does not migrate easily in groundwater, Al enrichment and Fe removal can occur only in acidic and reducing conditions with the presence of organic matter.

The geological and experimental studies show that "coal–bauxite–iron" structure in Lindai deposit is formed under certain hydrogeological conditions, i.e., since lateritic bauxite or Al-rich laterite deposited upon the semi-closed karst depressions, Si can be continuously removed out under neutral/acidic groundwater conditions; the coal/carbonaceous rock overlying the bauxitic materials were easily oxidized to produce acidic (H_2S, H_2SO_4, etc.) and reductant groundwater with organic materials that percolated downward, resulting in enrichment of Al in underlying bauxite; it also reduced Fe^{3+} to its easily migrating form Fe^{2+}, moving downward to near the basal carbonate culminated in precipitating of ferruginous (FeS_2, $FeCO_3$, etc.) strata of the "coal–bauxite–iron" structure. Thus, the bauxitic materials experienced Al enrichment and Si and Fe removal under above certain hydrogeological conditions forming the high-quality bauxite.

1. Introduction

Bauxite resources consist of economic concentrations of aluminum minerals such as gibbsite [$Al(OH)_3$], boehmite [γ-AlO(OH)], and diaspore [α-AlO(OH)] which are formed by alteration and weathering of precursor rocks that are rich in aluminosilicate. Bauxite deposits are generally divided into three types

* Corresponding authors at: Institute of Geochemistry, Chinese Academy of Sciences, 99th Linchengxi Road, Guiyang 550081, China.
E-mail addresses: zhuxqcas@sohu.com (X.-Q. Zhu), tanghaoshu@163.com (H.-S. Tang).

http://dx.doi.org/10.1016/j.oregeorev.2016.11.033
0169-1368/

according to their occurrence status and genesis, i.e., lateritic, tikhvin, and karstic type bauxites (Bárdossy, 1982; Bárdossy and Aleva, 1990). Lateritic type bauxites containing gibbsite as the main aluminum-rich mineral are formed by chemical weathering and is the main type of bauxite resources in the world (>90%) (Bárdossy, 1982; Bárdossy and Aleva, 1990). Tikhvin type bauxites that are detrital bauxite deposit overlying the eroded surface of aluminosilicate rocks and are the erosional product of lateritic bauxite deposits (Hanilçi, 2013; Zamanian et al., 2016). Karstic type bauxites, which contain diaspore and/or boehmite as the main aluminum-rich minerals, occur upon carbonate rocks and are formed by lateritic bauxite or Al-rich laterite deposition on karst depressions (Bárdossy, 1982). Established models of karstic bauxite generally show that the source materials, which are lateritic bauxites or Al-rich laterites derived from the chemical weathering of precursor rocks, form the bauxite deposits upon karst surfaces (karst depressions or sinkholes) (Clarke, 1966; Bárdossy, 1982; D'Argenio and Mindszenty, 1995; Öztürk et al., 2002; Liu et al., 2010; Wang et al., 2011a; Ling et al., 2013; Yu et al., 2014; Mongelli et al., 2016; Zamanian et al., 2016). The karstification plays a significant role in bauxite mineralization because it can develop large amount of voids (e.g., cavities) and basins (e.g., depressions and sinks) that host bauxites materials and provide excellent drainage conditions that conductive to bauxite formation (Bárdossy, 1982; Gao et al., 1992; MacLean et al., 1997; Laznicka, 2006; Zarasvandi et al., 2012; Zamanian et al., 2016). The bauxite deposits in China are mainly found in the Guizhou, Guangxi, Shanxi, and Henan Provinces. Guizhou's reserves consisted of 155.23 million tons, by the end of 2008 (USGS, 2009; Gu et al., 2013a,b; Ling et al., 2013, 2015). The bauxite deposits in Guizhou are mainly karstic type and are divided into the following five ore belts from south to north separated by unmineralized areas (highland): the Xiuwen, Xifeng, Zunyi, Zhengan, and Daozhen ore belts (Fig. 1). The Xiuwen, Xifeng, and Zunyi ore belts are located in the Central Guizhou Province; the Zhengan and Daozhen ore belts are located in the Northern Guizhou Province (Gu et al., 2013a,b; Ling et al., 2013; Weng et al., 2013; Zhang et al., 2013).

Many bauxite deposits worldwide occur associated with coal or black carbonaceous rocks and ferroan strata, forming a "coal–bauxite–iron" structure (Kalaitzidis et al., 2010; Ling et al., 2013; Zhang et al., 2013, and references therein). In which, the Al-bearing rock series are consisted of three segments (i.e., iron argillite, bauxite, and coal layers) ordered from the lower to the upper segments of the profile (Zhang et al., 2013). This structure has been discovered in many karstic bauxite deposits around the world, e.g., the Ghiona bauxite deposit in Greece (Kalaitzidis et al., 2010), the Nurra bauxite deposit in Italy (Mameli et al., 2007), the Kanisheeteh bauxite deposit in Iran (Calagari and Abedini, 2007). Moreover, the karstic bauxite deposits in China (e.g., Guizhou, Henan, Shandong, and Liaoning Provinces) are frequently sandwiched with overlying coal layers and underlying ferruginous strata and formed a "coal–bauxite–iron" special structure (Bárdossy, 1982; Beneslavsky, 1974; Yang et al., 2011; Ling et al., 2013, 2015; Liu and Liao, 2013). For instance, the overlying strata of karstic bauxite deposits involved in the Upper Carboniferous Benxi Formation are the main coal beds in North China, while the underlying strata are "Shanxi-type" iron deposits. And the karstic bauxite deposits in the Lower Carboniferous Jiujialu Formation in Guizhou Province, SW China, where the upper segment consists of coal beds/black carbonaceous rocks, and the lower segment is characterized by "Qingzhen-type" iron deposits/ferruginous strata (Yang et al., 2011; Ling et al., 2013; Liu and Liao, 2013). Above examples indicate that the bauxite ores were highly associated with "coal–bauxite–iron" structure. Study in-depth this interesting structure is necessary, and will provide important insights into our understanding of the mineralization of karstic bauxite deposits.

The mobility of elements during bauxitization has been studied for decades (Patterson, 1967; MacLean et al., 1997; Valeton et al., 1987; Öztürk et al., 2002; Laskou and Economou-Eliopoulos, 2007, 2013; Calagari and Abedini, 2007; Mameli et al., 2007; Wang et al., 2011a; Zarasvandi et al., 2012; Abedini and Calagari, 2013; Gu et al., 2013a; Hanilçi, 2013; Mongelli et al., 2014, 2016; Yu et al., 2014; Zamanian et al., 2016). The most important conclusion obtained in these studies is that the enrichment of Al and the removal of Si and Fe are the key factors in karstic bauxite formation. For instance, Mameli et al. (2007) investigated the mineralogical characteristics of the Nurra bauxite deposit in Sardinia, Italy, and determined that the bauxitization process proceeded from the down surface with the accumulation of Al_2O_3 and TiO_2 and the loss of Fe_2O_3 and SiO_2. Similarly, the occurrence of high-grade ores in the Parnassos-Ghiona bauxite deposit in Greece resulted from Fe-leaching during/after bauxite formation (Laskou and Economou-Eliopoulos, 2013, and references therein). Very few studies, however, have used experimental methods to investigate the mobility of elements and the genesis of bauxite during bauxitization. Only Valeton (1972) and Chen (1991, 1996) conducted such experiments; they indicated that acidic conditions are conducive to silicon and aluminum fractionation, and that humic acid can enhance the migration of colloidal SiO_2, Fe_2O_3, and Al_2O_3 in water (Valeton, 1972; Chen, 1991, 1996).

Therefore, this study reports the geological and geochemical characteristics of Lindai karstic bauxite deposit, which is one of the most representative bauxite deposits in the Xiuwen ore belt, Central Guizhou Province, Southwest China, and conduct the simulated weathering experiments (soaking and leaching experiments) on the modern laterite of the parent rocks of bauxite. Based on these experiments, we attempted to simulate the most suitable hydrogeological conditions for Si and Fe migration along with Al enrichment during the formation of karstic bauxites. These conditions would help us to gain a better understanding of the hydrogeological conditions of ore-forming processes and provide a theory of bauxite mineralization.

2. Geological features

The research area, which is near the southern margin of the Yangtze Plate (Fig. 1a), lies in the Guiyang Complex Tectonic Deformation Zone, North Guizhou Anticline, Yangtze Paraplatform, China (Guizhou Provincial Bureau of Geology and Mineral Resources, 1987). The bauxite deposits in Central Guizhou Province are combined controlled by the Central Guizhou anticlinorium and Ziyun-Yadu (ZY) and Puding-Guiyang-Huangping (PGH) Faults, which strictly limited the distribution of the central Guizhou bauxite to the southern anticlinorium, the northern PGH Fault and the eastern ZY Fault (Gao et al., 1992; Fig. 1b). The Zunyi and Xifeng ore belts are located in the northern limb of the anticlinorium, whereas the Xiuwen ore belt is located in the southern limb of the anticlinorium (Gao et al., 1992; Fig. 1b). The exposed rocks in the Xiuwen ore belt are primarily carbonates, and the landscape is a typical karst landform made up of low and rolling hills.

The Lindai deposit, that belongs to the Xiuwen ore belt deposited in Lindai village, Guiyang City, Guizhou Province, SW China (Figs. 1 and 2), includes two ore bodies: Weijiazhai and Muzhuchong. The Weijiazhai ore body has a length of 1350 m, a width of 300–400 m, and a thickness of 0.5–15.3 m (general 2–7 m). The Muzhuchong ore body has a length of about 1000 m, a width of 350 m, and a thickness of 0.61–7.23 m (2.6 m on average). The ore body is hosted by the Lower Carboniferous Jiujialu Formation which displays unconformable contacts with the overlying and underlying lithologies (Figs. 2 and 3). The underlying stratum includes the Middle Cambrian Shilengshui Formation dolomite (Figs. 2c and 3), which is the

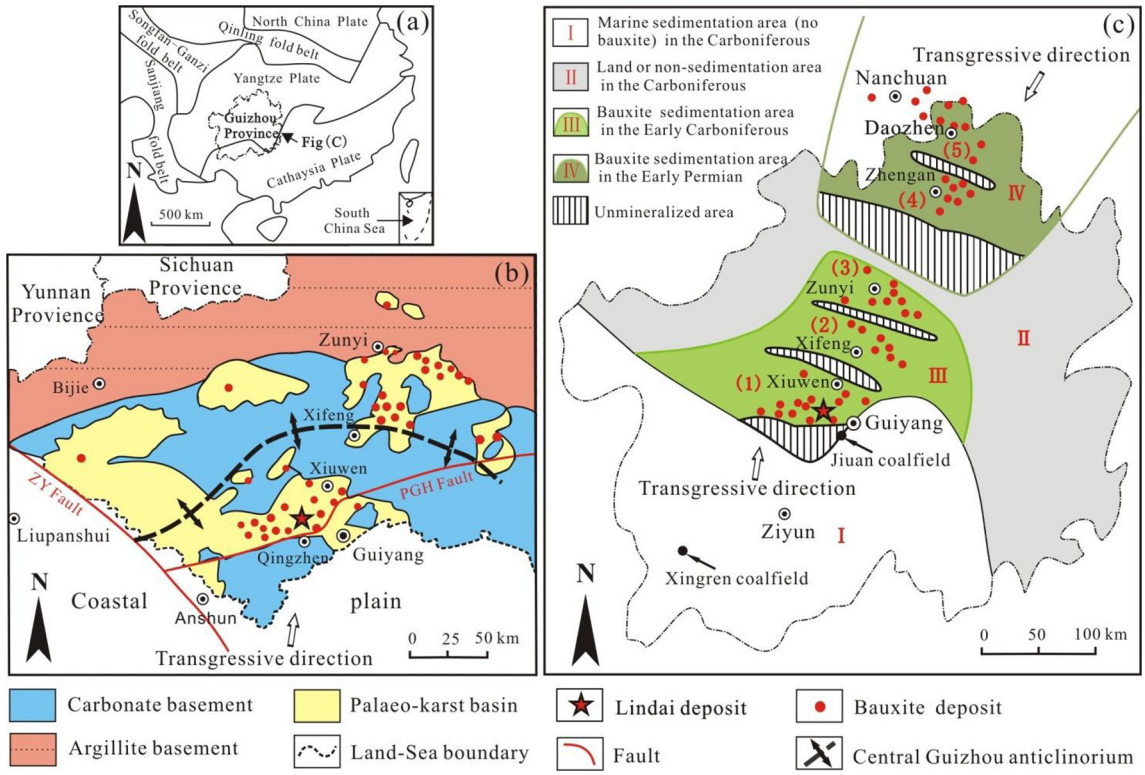

Fig. 1. (a) Inset map of the Yangtze Plate showing the location of the research area. (b) paleogeomorphologic map of the central Guizhou district during the deposition of Al-bearing rock series (Jiujialu Fm.) (after Gao et al., 1992). ZY fault: the Ziyun-Yadu fault; PGH fault: the Puding-Guiyang-Huangping fault. And (c) paleogeomorphologic map of the central and northern Guizhou district during Al-bearing rock series deposition (after Gao et al., 1992). (1) Xiuwen ore belt, (2) Xifeng ore belt, (3) Zunyi ore belt, (4) Zhengan ore belt, and (5) Daozhen ore belt.

precursor rock of the Lindai Al-bearing rock series (Bárdossy, 1982; Ling et al., 2013). The overlying stratum comprises the Lower Carboniferous Baizuo Formation Limestone (Figs. 2c and 3). The Jiujialu Formation, which has inverted bedding with nearly south–north strike and NNE inclination with a dip angle of 70–80°, exhibits a typical "coal–bauxite–iron" structure that is divided into three segments (Fig. 2c and 4): (1) the upper segment consists of coal layers interbeded with clay stone and black carboniferous shale with thickness ranging from 3 to 4 m (Figs. 2c and 4b); (2) the middle segment consists of bauxite layers with thickness ranging from 0.5 to 15.3 m (general 5–6 m); and (3) the lower segment consists of iron layers that are primarily composed of red, steel gray, or dark ferruginous clay and iron rock with thickness ranging from 2 to 10 m (Fig. 4c and d) (Ling et al., 2013).

The Jiuan and Xingren coal mines are located at Guiyang city, Guizhou Province and Southwest of Guizhou, respectively (Fig. 1c). Both coal mines are hosted by the Upper Permian Longtan Formation. The Jiuan coal including 5–6 coal layers with total thicknesses of 6.5–8.8 m. The pit water is mostly colorless, but a sedimentary layer of reddish-brown ferric materials is observed at the bottom of the tunnel. The Xingren coalfield has a total output of raw coal of about 2.5–3.0 million tons every year, and the utilized coal layers have a total thickness of about 12 m. The bedrock is mainly composed of carbonate rocks with the age of Permian–Triassic periods (Wu et al., 2009).

3. Sampling and experimental methods

3.1. Sampling and analytical methods

3.1.1. Sampling

All samples were collected from profile outcrops and open pits. Five samples (i.e., LD-1, 2, 3, 4, and 5) were collected from a well-exposed cross-section of the Weijiazhai ore body (Fig. 2c), and the other four samples (i.e., LD-7, 8, 9, and 10) were collected from an open pit of the Muzhuchong ore body (Fig. 4). The dolomite basement (i.e., LD-13) and the laterite samples (i.e., LD-11 and 12) were collected from a relatively complete laterite profile located about 300 m from the cross-section (Fig. 2a and b).

Because it was impossible to collect the paleo-laterite of the Lindai bauxite (paleo-laterites have been transformed to the Jiujialu Formation Al-bearing rock series during bauxite formation period, i.e., the early Carboniferous), modern laterite sample (LD-12) that weathered from the precursor rock of bauxite (Middle Cambrian Shilengshui Formation dolomite) were collected to conduct simulated weathering experiments. Evidently, modern laterite and paleo-laterite have some differences in element and mineral compositions because they formed in the different weathering characteristics (mainly the climates). Fortunately, the aim of the experiments was to simulate the hydrogeological conditions of the bauxitization process after the laterites were deposited on karst surfaces. In addition, the modern laterite and paleo-laterite have similar mineral compositions consisting of quartz, illite, hematite, kaolinite, and smectite. (e.g., Clarke, 1966; Bárdossy and Aleva, 1990; Anand et al., 1991; Boulangé et al., 1996; Meyer et al., 2002; Ji et al., 2004; Ma et al., 2007; Smith, 2009; Horbe and Anand, 2011). Therefore, even though the distinctions between paleo-laterite and modern laterite should not be ignored in the experimental process, the use of modern laterite as an experimental sample to investigate the relationship between the mobility of Al, Si, and Fe during the bauxite formation is both meaningful and necessary.

3.1.2. Analytical methods

Trace and REE element abundances were analyzed by quadrupole inductively coupled plasma mass spectrometry (ICP-MS; PerkinElmer, ELAN DRC-e). The sample (50 mg, 200 mesh) was placed

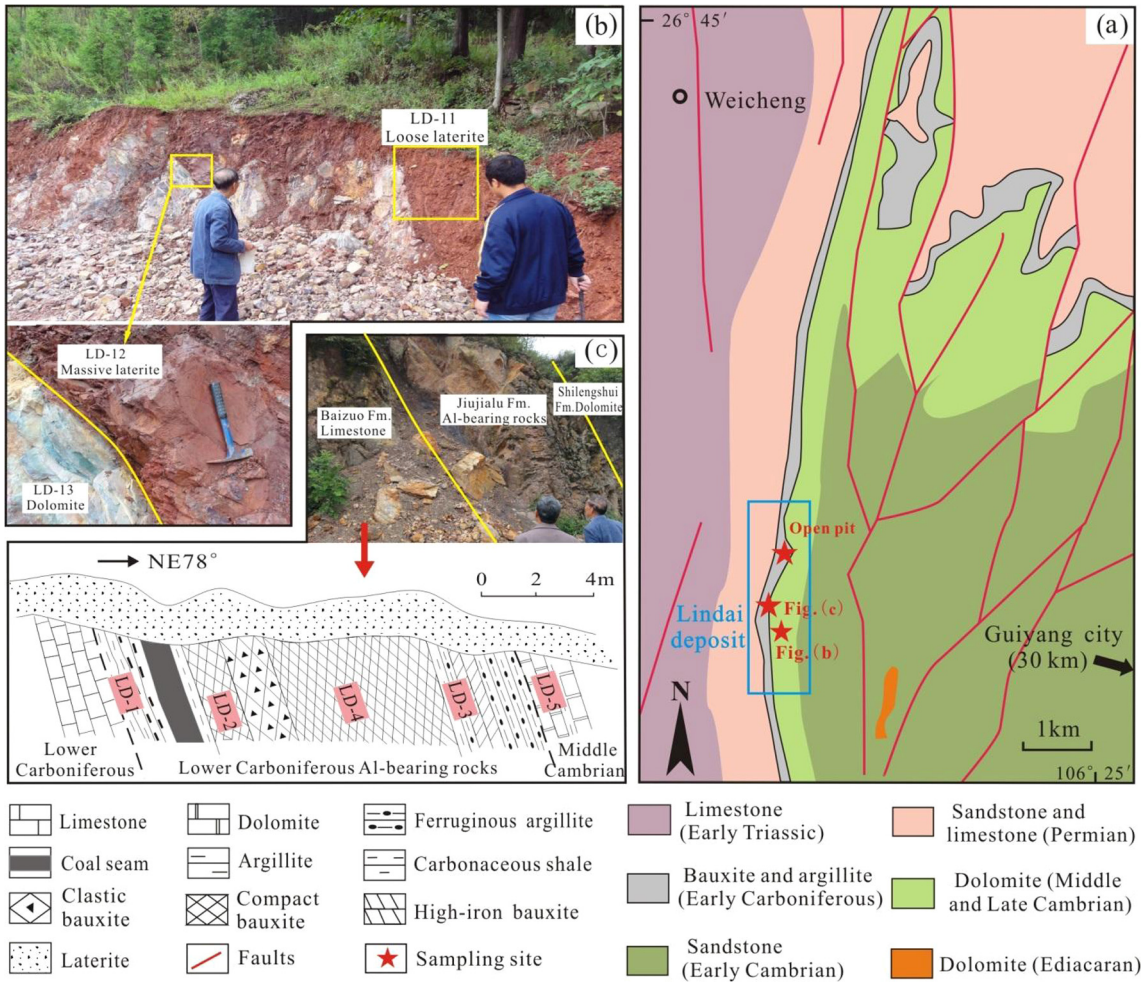

Fig. 2. (a) Geological features of the Lindai bauxite deposit, Guiyang, Guizhou Province, China (after the 1:200,000 map of geological and mineral resources, P. R. China, 1969); (b) characteristics of the laterite profile; and (c) geological cross-section of the Lindai bauxite deposit.

in a Teflon beaker, and 1 mL each of HF and HNO_3 was added. The beaker was set in a steel sleeve and placed on an electrothermal constant-temperature dry box (190 °C) for 24 h until the sample was completely dissolved. The sample was then air-dried. This process was repeated with 0.5 mL HNO_3. Subsequently, 0.5 mg Rh was added to the desiccated sample as the internal standard along with 2 mL HNO_3 and an appropriate volume of ultrapure water. The solution was then heated in an electrothermal constant-temperature dry box (190 °C) for 5 h to ensure that all substances had completely dissolved. This solution (0.4 mL) was then transferred to a centrifuge tube, and ultrapure water was added to yield a final volume of 10 mL. The tube was retained for ICP-MS analysis. The ICP-MS measurement was monitored by the international standard samples OU-6, AMH-1, and GBPG-1 (Potts et al., 2000, 2001; Thompson et al., 1999), and trace element concentrations were calibrated by the recovery rate of the standard samples. The detection limits were 0.01 ppm and the relative standard deviation (RSD) in the trace and REE element analysis were below 10%. The analytical procedures are detailed by Franzini et al. (1972) and Qi et al. (2000), and the results are summarized in Table 1.

The major element abundances of the samples were measured by X-ray fluorescence (XRF) (PANalytical, AXIOS-PW4400). The samples were crushed to 200 mesh in a mortar. Next, 0.7 g of the crushed sample was mixed with 7 g of composite flux ($Li_2B_4O_7$:$LiBO_2$:LiF = 4.5:1:0.4) in a platinum crucible and heated to 1150 °C in a melting chamber. Once the sample was liquefied, it was analyzed by XRF after cooling and solidification. The detection limits were about 0.01 wt.% and the analytic results are summarized in Table 1. The mineral components were analyzed by X-ray diffraction (XRD; Dmax/2200; Japan) operating under the following conditions: at 40 kV and 20 mA; scanning scope, step length and speed were set to 2–60°, 0.04° and 10°/min, respectively. The XRD measurements were monitored by the instrument standard Cu Kα target, and semi-quantitatively calculated by the K value method (Mordberg et al., 2000). Inductively coupled plasma optical emission spectrometry (ICP-OES, Model Vista MPX produced by Varian Company) was utilized to determine the soaking and leaching solution compositions. The ICP-OES measurement was monitored by external standard samples, and the RSDs for the Al, Si, and Fe analyses were below 10%. The ion composition of coal pit water was determined by ion chromatography (Model ICS90 produced by Dionex Company). The pH and Eh values of the solution were determined using a Seven Easy S20k laboratory pH meter (Produced by Mettler Toledo) with pH electrode (Model InLab Expert Pro) and ORP platinum electrode (Model 301Pt-C). All analyses were conducted at the Institute of Geochemistry, Chinese Academy of Sciences.

3.2. Simulated weathering experiments

3.2.1. Leaching experiments

Leaching experiments were conducted using an automatic cycle leaching device (Fig. 5) composed of a gas generating device and an automatic cycle leaching device. The latter consists of three parts:

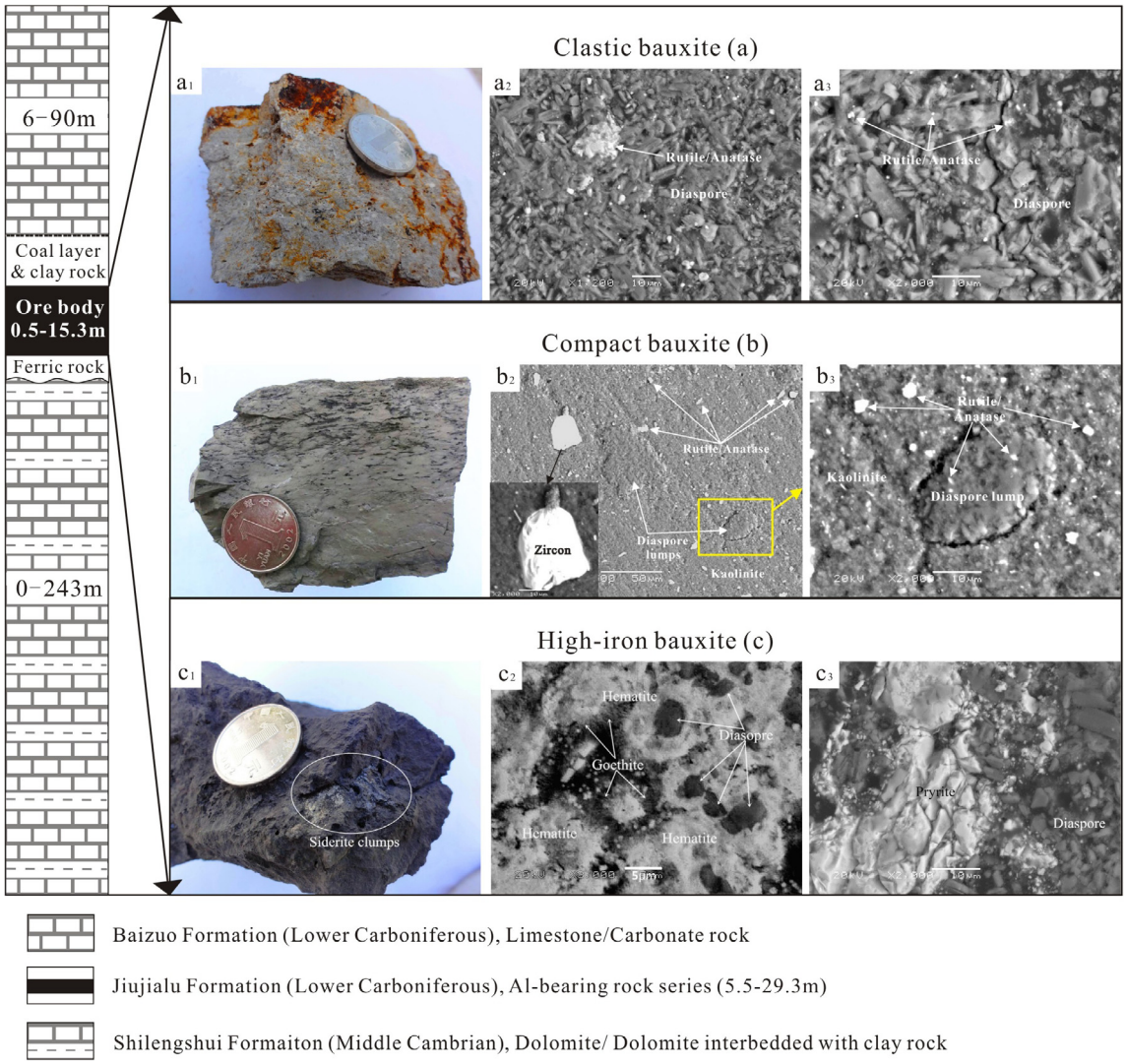

Fig. 3. Stratigraphic column of the Lindai bauxite profile with macro and backscattered electron (BSE) images of bauxite samples. Specimen and BSE images of (a) the clastic bauxite; mineral compositions are dominated by short prismatic or platy shape (2–10 μm) diaspores with minor debris minerals of rutile/anatase. (b) The compact bauxite; diaspore lumps (10–50 μm), zircon and rutile/anatase are scattered within kaolinite matrix, and the irregular granular diaspore particles (0.1–1 μm) with a xenomorphic structure. (c) The high-iron bauxite with siderite clumps; diaspore, pyrite, hematite, and goethite are coexisting. Actually, granular diaspore cores are cemented by hematite, followed by secondary goethite (c_2).

weathering and leaching, evaporation cycle, and rainwater synthesis. The specific experimental procedures are as follows: (1) the massive laterite (LD-12) was smashed (Fig. 2b), and some 8–20 mesh samples were selected using a standard sieve. The samples were washed three times with running water and then with ultrapure water followed by drying in a 60 °C oven for 8 h. The massive laterite samples were then weighed in sextuplicate (each weighing 130 g) using a balance and loaded in the glass column at the weathering and leaching part. (2) The gas generation device was composed of an air generator and a wide-mouthed jar containing a solution of HCl (a nonreducing inorganic acid), HNO_3 (an oxidizing inorganic acid), HBr (a weak reducing inorganic acid), oxalic acid (a strong reducing organic acid), citric acid (a weak reducing organic acid) and humic acid (a mixed organic acid). During operation, air from the air generator went in the wide-mouthed jar, where it mixed with the acids; the acid-containing air then entered the automatic cycle leaching device. (3) The electric stove power should be controlled to sustain the same rate of evaporation in the flask above the electric stove. Water vapor moves from the flask into the rainwater synthesis part, mixes with the six acid-containing gases, and condenses to rainwater with similar pH values (pH range from 2 to 3) to leach the sample columns (Table 2). The leaching experiment continued 8 h a day for 15 days at a rate of approximately 7 mL of leaching solution per minute. The "rainwater" was controlled to 2200–2800 mm up and down, about two times the annual average rainfall in Guiyang city (1200–1500 mm) (Compilation of the annual average rainfall in China for 30 years).[1] (4) Samples of 10 mL were taken from the flask every three days for analysis after maintaining the solution volume of 400 mL. Subsequently, installing a new flask with 400 mL distilled water and then conducts next step of the experiment. The solutions were centrifuge filtered through a pinhole membrane, and 0.5 mL HNO_3 was added to each sample solution for acidification followed by analysis with ICP-OES. The results of the analysis are shown in Table 2.

3.2.2. Soaking experiments

Soaking experiments were conducted on the modern laterite sample (LD-12) (Fig. 2b). Samples of 20–60 mesh size (5 g) were immersed in the test tube. To each of these, 50 mL of preparation

[1] Data provided by the China Meteorological Data Sharing Service System (http://cdc.cma.gov.cn/).

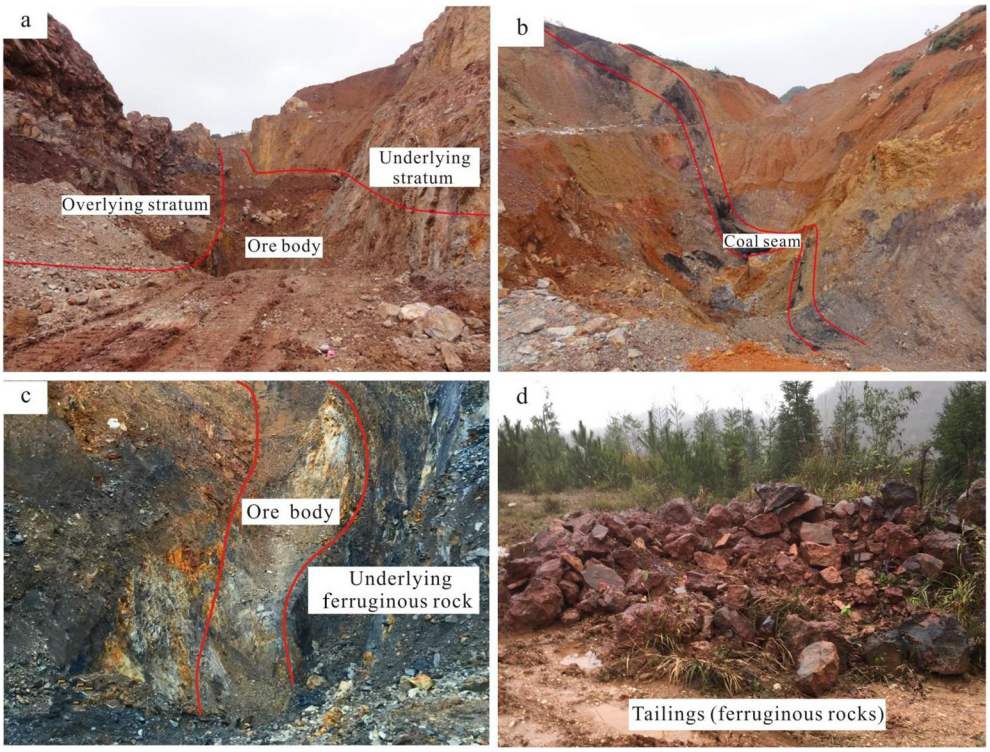

Fig. 4. Field photographs illustrating the ore body features of the Lindai bauxite deposit, Central Guizhou Province, China. (a) Muzhuchong open pit at the Lindai deposit; (b) coal seam on the top of the bauxite ore body; (c) ferruginous rock and overlying bauxite ore; and (d) tailings, mainly ferruginous rock.

solution containing ascorbic acid (a strong reducing organic acid), HNO_3, HBr, or humic acid was added. The pH of the solutions was adjusted to specified values using HCl and NaOH solutions, and the test tubes were then closed with glass covers. Thirty days later, 12 mL of the sample solution was removed, centrifuged, and filtered through a pinhole membrane. HNO_3 (0.5 mL) was then added to this solution for acidification followed by ICP-OES analysis. The analysis results are shown in Table 3.

3.2.3. Method of data processing

Because the massive laterite sample (LD-12) has different contents of Al_2O_3, SiO_2, and Fe_2O_3, the elemental (Al, Si, or Fe) concentrations of the soaking or leaching solutions (ppm) could not completely express the migration relationship between these three elements. Therefore, the element migration rate (K_x) was thus calculated by the formula:

$$K_x = (a_x \cdot V)/A_x \cdot M$$

where a_x is the concentration of the soaking or leaching solution (ppm), V is the total volume of the soaking or leaching solution (mL), A_x is the abundance (%) of elements in the laterite sample (LD-12), and M is the weight (g) of the rock sample. Therefore, $a_x \cdot V$ is the total quantity (μg) of elements (Al, Si, or Fe) in the leaching or soaking solution and $A_x \cdot M$ is the total quantity (g) of elements (Al, Si, or Fe) in the experimental sample (massive laterite, 130 g in leaching experiments and 5 g in soaking experiments). The specific meaning of K_x is the quantity (μg) of element (Al, Si, or Fe) migrated per gram of that element in massive laterite during the experiment.

4. Results

4.1. Texture and mineralogy

Based on texture and iron abundances, the bauxite commonly consist of clastic, compact, and high-iron ores in the Lindai deposit (Fig. 3a, b, and c). In upward order, the high-iron ore occurs at the foot wall of the profile. It usually has brown or black color (Fig. 3c) and mainly clastic texture. The compact ore overlies the high-iron ore and makes the main ore bedding. It is gray, slippery, and exhibits a pelitomorphic texture with a conchoidal fracture (Figs. 2c and 3b). The clastic ore occurs mainly in the middle segment of the profile. It is in gradual transition from the compact ore and exhibits a clastic texture (Figs. 2c and 3a). In addition, loose laterite (LD-11) shows loose texture, whereas massive laterite (LD-12) shows massive texture (Fig. 2b).

The SEM and XRD analyses of the bauxite samples show that the Lindai bauxite ores comprise diaspore, boehmite, kaolinite, illite, smectite, hematite, and a small amount of detrital minerals such as rutile and zircon (Table 4; Fig. 3). As with many other bauxite deposits throughout the world, diaspore and/or boehmite are the main economic minerals of aluminum in the Lindai deposit (Mongelli, 1997; Laskou and Economou-Eliopoulos, 2007; Liu et al., 2012; Wang et al., 2012; Boni et al., 2013; Gu et al., 2013a; Mongelli et al., 2014). Two red laterite samples primarily comprise quartz, illite, hematite, dolomite, kaolinite, and smectite (Table 4). In addition, loose laterite (LD-11) shows loose texture, whereas massive laterite (LD-12) shows massive texture (Fig. 2b).

The diaspore particles (2–10 μm) in clastic ore commonly have hypautomorphic crystal structures and exhibit short prismatic or platy shapes (Fig. 3a). As for high-iron ore, it includes high contents of siderite, pyrite, or hematite (Figs. 2c and 3c). Granular diaspores are mainly cemented by hematite, and followed by goethite (Fig. 3c_2). The cores of diaspore usually exhibit middle to well-rounded shapes (Fig. 3c), indicate that it was transported over extensive distances by the surface water. In compact ore, diaspores (0.1–1 μm) often have xenomorphic structures and exhibit irregular shapes (Fig. 3b). Diaspore lumps with different shapes are scattered within the kaolinite matrix in the sample of LD-9 (Fig. 3b). Debris minerals such as rutile and anatase inside the diaspore lumps may suggest that diaspore lumps and rutile and anatase formed synchronously. The differences in texture between the

Table 1
Major (wt.%), trace, and REE (ppm) element compositions of selected samples from the Lindai Al-bearing rock series and laterite profile (LD-7, 8, 10, 11, 12, and 13 from Ling et al., 2013).

Sample No.	LD-1	LD-2	LD-3	LD-4	LD-5	LD-7	LD-8	LD-9	LD-10	LD-11	LD-12	LD-13
Lithology	Clay	Compact bauxite	Ferruginous clay	Bauxitic clay	Dolomite	Clastic bauxite	Bauxitic clay	Compact bauxite	High iron bauxite	Loose laterite	Massive laterite	Dolomite
SiO_2	43.1	27.4	35	34.1	0.49	1.2	34.5	26	1.53	36.3	40.3	2.13
Al_2O_3	32.8	53	31.8	46.2	0.38	76.8	44.9	53.2	70.9	21.5	21.6	1.5
Fe_2O_3	7.31	1.12	18.4	1.36	0.62	2.18	2.2	1.07	6.29	14	15.7	0.74
MgO	0.68	0.23	0.16	0.63	20.7	0.15	0.51	0.51	0.21	4.26	4.2	19.4
CaO	0.06	–	–	–	30.5	–	–	–	–	2.62	0.68	29.7
Na_2O	–	–	0.08	0.3	–	0.74	0.06	0.93	1.22	0.2	0.72	0.89
K_2O	4.83	0.59	0.52	3.52	0.1	0.14	1.23	1.12	0.19	5.13	6.33	0.33
MnO	–	–	–	–	0.06	–	0.02	–	–	0.18	0.05	0.04
P_2O_5	0.01	0.04	0.02	0.06	0	0.23	0.07	0.02	0.13	0.1	0.27	0.03
TiO_2	1.37	3.65	2.22	2.55	0.02	5.12	3.58	3.5	2.55	0.86	1.2	0.07
L.O.I.	10.1	14.5	12	12.1	47.2	14.3	13.5	14.4	17	13.7	8.03	45.2
Total	100	100.6	100.1	100.7	100	100.9	100.5	100.8	100	98.9	99	100
Ki	2.34	0.92	1.96	1.31	2.3	0.03	1.37	0.87	0.04	3.01	3.32	2.53
CIA	87	98.9	98.2	92.4	1.23	98.9	97.2	96.3	98.1	73	73.6	4.63
Cr	120	112	133	102	74.8	106	96.3	94.3	60.6	122	162	181
Ni	18.8	56	26.3	180	70.1	210	103	114	145	170	297	225
Zr	288	806	620	648	5	1890	1180	1280	1240	222	512	19.3
Hf	7.98	23.3	18.1	18.2	0.11	51.9	32.3	36.2	33.8	6.42	14.2	0.52
Nb	30.7	75.3	44.5	53.7	0.46	117	89	75.5	66.9	22	29.4	1.89
Ta	2.56	6.36	3.8	4.4	0.05	5.19	4.81	6.24	3.76	1.56	1.76	0.28
La	45	45.4	61.3	146	1.62	39.1	82.8	51.3	43.5	81	93.3	4.64
Ce	84.6	85.6	120	278	3.32	85.4	140	93.1	44.7	164	203	8.6
Pr	8.63	8.54	12.7	35.7	0.36	8.98	15.4	9.87	9.03	19	21	1.13
Nd	31.8	26.8	46.3	131	1.26	37.8	55.3	34.3	33.1	72	76.6	4.55
Sm	8.31	4.92	14.9	20	0.5	9.18	11.8	7.37	7.83	16.1	15.2	1.03
Eu	1.95	0.83	3.16	3.11	0.13	1.91	2.19	1.47	1.39	3.04	3.03	0.19
Gd	8.78	4.47	13.4	14.3	0.63	13.8	11.5	8.04	17.7	15.5	14.8	1.12
Tb	1.61	0.92	2.4	2.36	0.12	2.6	1.95	1.64	3.81	2.54	2.24	0.17
Dy	8.7	5.86	12.3	11.8	0.65	14.1	11.8	9.99	22.2	14.8	12.1	0.99
Ho	1.88	1.31	2.38	2.47	0.15	2.58	2.49	2.1	4.1	2.86	2.41	0.18
Er	5.16	3.94	6.23	6.97	0.29	6.99	7.74	6.21	10.5	8.46	7.12	0.49
Tm	0.79	0.61	0.92	1.08	0.05	0.95	1.15	1.02	1.32	1.2	0.96	0.06
Yb	4.62	4.27	5.64	6.84	0.3	5.96	7.95	6.93	7.67	8.26	6.44	0.38
Lu	0.72	0.61	0.82	1.03	0.04	0.83	1.18	1	0.981	1.17	0.93	0.06
Y	46.6	34.6	49.4	58.9	4.28	71.7	56.6	51.8	116	72.9	64.4	5.35
∑REE	213	194.1	302.4	660.6	9.42	230.2	353.3	234.3	207.8	409.9	459.1	23.6
∑LREE	180	172.1	258.4	613.8	7.19	182.4	307.5	197.4	139.5	355.1	412.1	20.1
∑HREE	32.3	22	44.1	46.8	2.23	47.8	45.8	36.9	68.3	54.7	47	3.44
LR/HR	5.59	7.82	5.86	13.1	3.22	3.81	6.72	5.35	2.04	6.49	8.77	5.8
Ce/Ce^*	1.05	1.07	1.05	0.94	1.07	1.12	0.96	1.01	0.55	1.02	1.12	0.92
Eu/Eu^*	0.7	0.54	0.68	0.56	0.71	0.52	0.58	0.58	0.36	0.59	0.62	0.53
Y/Ho	24.8	26.4	20.8	23.8	28.9	27.8	22.7	24.7	28.3	25.5	26.7	30.2
Zr/Hf	36.1	34.6	34.3	35.6	45.9	36.4	36.5	35.4	36.7	34.6	36.1	37.3
Nb/Ta	12	11.8	11.7	12.2	9.82	22.5	18.5	12.1	17.8	14.1	16.7	6.72
La/Y	0.97	1.31	1.24	2.48	0.38	0.55	1.46	0.99	0.38	1.11	1.45	0.87

Notes: $CIA = Al_2O_3/(Al_2O_3 + CaO + Na_2O + K_2O) \times 100$; $Ki = (SiO_2/Al_2O_3 \times 1.78)$; $Ce/Ce^* = Ce_N/(La_N \cdot Pr_N)½$; $Eu/Eu^* = Eu_N/(Sm_N \cdot Gd_N)½$.

kaolinite matrix and the diaspore lump (Fig. 3b) indicates that the precursor material of the lump was most likely gibbsite, which was inherited from the laterite lump that formed in the process of chemical weathering. Because the gibbsite was the main aluminum mineral in laterite bauxite and diaspore/boehmite rarely occurred (Beneslavsky, 1974; Grubb, 1979; Bárdossy, 1982; Meyer et al., 2002; Hanilçi, 2013). Accordantly, gibbsite lumps within laterite deposited on the karst depression after an extensive diagenesis process and transformed to boehmite/diaspore in suitable conditions.

4.2. Geochemistry

4.2.1. Major elements geochemistry

The Ki factor [$Ki = (SiO_2/Al_2O_3) \times 1.78$] plays an important role in bauxite classification (Valeton, 1972; Al-Bassam, 2005). Five classes were defined by Valeton (1972): (1) $Ki < 0.2$ indicates high-quality bauxite; (2) $0.2 < Ki < 0.5$ indicates low-quality bauxite; (3) $0.5 < Ki < 1.0$ indicates kaolinitic bauxite; (4) $1.0 < Ki < 1.5$ indicates bauxitic clay; and (5) $Ki > 1.5$ indicates clay. Based on the criterion mentioned above, the samples LD-7 and LD-10 are high-quality bauxites as their Ki values are 0.03 and 0.04, respectively. LD-2 and LD-9 are kaolinitic bauxites because their Ki values are 0.92 and 0.87, respectively. LD-4 and LD-8 are bauxitic clay due to their high Ki values (1.31 and 1.37, respectively), and LD-1 and LD-3 belong to the clay stone category with Ki values of 2.34 and 1.96, respectively (Table 1). The Al_2O_3 contents of the bauxite samples range from 53.0 wt.% to 76.8 wt.% (average 63.5 wt.%). The Fe_2O_3 content in Al-bearing rocks ranges from 6.29 wt.% to 1.07 wt.%. And the two high-quality bauxite samples have the lowest SiO_2 contents (i.e., 1.20 wt.% and 1.53 wt.%). However, two laterite samples (LD-11 and 12) show high contents of Al_2O_3 (21.5 and 21.6 wt.%), SiO_2 (36.3 and 40.3 wt.%), Fe_2O_3 (14 and 15.7 wt.%), CaO (2.62 and 0.68 wt.%), and MgO (4.26 and 4.2 wt.%), respectively (Table 1). Evidently, SiO_2 and Fe_2O_3 contents must be removed if the modern laterite converts to high-quality karstic bauxite.

4.2.2. Trace and rare earth elements (REEs) geochemistry

Compositions of trace elements and rare earth elements (REE) of the bauxite ores and underlying carbonates are presented in

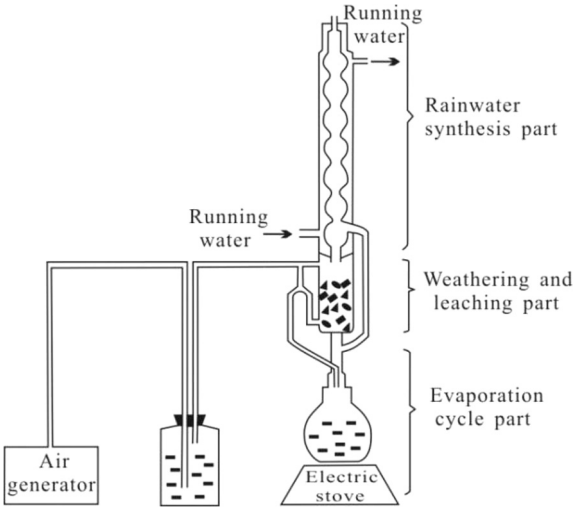

Fig. 5. Schematic diagram of the leaching device.

Table 1. It shows that ∑REE ranges from 23.58 to 459.12 ppm (average of 280.65 ppm) in these samples (Table 1). The light rare earth elements (LREEs; La, Ce, Pr, Nd, Pm, Sm, Eu) are significantly enriched compared to heavy rare earth elements (HREEs; Gd, Tb, Dy, Ho, Er, Tm, Yb, Lu). LREE/HREE = 2.04–8.77, and the ore-bearing rock series and the underlying Middle Cambrian Shilengshui Formation dolomite present similar REE patterns which are characterized by a regular decrease from La to Lu (Fig. 6). The values of Ce/Ce* are range from 0.94 to 1.12 (with average of 1.03) with the exception of LD-10 (Ce/Ce* = 0.55). The values of Eu/Eu* are range from 0.52 to 0.71 (with average of 0.55) with the exception of LD-10 (High-iron bauxite; Eu/Eu* = 0.36). The La/Y ratios in samples of the Lindai bauxite profile are range from 0.38 to 2.48 (Table 1). The Y/Ho ratios are 20.8 and 28.9 in ore-bearing rocks, similar to those of 28.9 and 30.2 in dolomite samples. The Zr/Hf ratios are 45.9 and 37.3 in dolomite samples and similar to those of ore-bearing rocks (34.3–36.7). The Nb/Ta ratios are 9.82 and 6.72 in dolomites, which lower than those of ore-bearing rocks of 11.7 to 22.5 (Table 1).

4.3. Characteristics of pit water

Pit waters from the Jiuan coal mine tunnel were strongly acidic (pH = 2.81–2.98) and had a high total iron concentration of 1273–1348 ppm. The Fe^{2+} concentration was 971–1258 ppm, accounting for more than 80% of the total iron. Si and Al were also high, reaching 186 and 298 ppm, respectively. The pit water also had high contents of SO_4^{2+} (5887–6838 ppm), Ca (528 ppm), and Mg (271 ppm) (Table 5).

4.4. Simulated weathering experiments

4.4.1. Leaching experiments

The concentrations and the migration rates of Al, Si, and Fe in organic acid conditions, especially in reducing ones are higher than those in inorganic acid conditions (Fig. 7). Among the inorganic

Table 2
Concentrations of leaching solutions in laterite leaching experiments on the Lindai bauxite deposit.

Experiment name	Characteristic of solution	Sample number	Al (ppm)	SiO_2 (ppm)	Fe (ppm)	K_{Al} (ug/g)	K_{Si} (ug/g)	K_{Fe} (ug/g)	K_{Si}/K_{Al}	K_{Fe}/K_{Al}
HCl leaching experiment (pH = 2.71, Eh = 481)	150 mL HCl + 150 mL distilled water	HCl-1	2.6	53.2	1.12	70	407	31.4	5.81	0.45
		HCl-2	2.6	27.5	0.38	70	210	10.6	3	0.15
		HCl-3	23.4	136	1.63	630	1039	45.7	1.65	0.07
		HCl-4	3.19	49	0.79	85.9	374	22.1	4.35	0.26
		HCl-5	5.52	32	1.55	149	245	43.4	1.64	0.29
		Average	7.46	59.5	1.09	201	455	30.6	–	–
HNO3 leaching experiment (pH = 2.56, Eh = 458)	150 mL HNO_3 + 150 mL distilled water	HNO_3-1	3.8	52.7	0.93	102	403	26.1	3.95	0.26
		HNO_3-2	3.28	35	0.73	88.3	267	20.5	3.02	0.23
		HNO_3-3	1.45	25.9	0.45	39	198	12.6	5.08	0.32
		HNO_3-4	1.92	16.8	0.64	51.7	128	17.9	2.48	0.35
		HNO_3-5	2.23	16.7	0.83	60	128	23.3	2.13	0.39
		Average	2.54	29.4	0.72	68.2	225	20.1	–	–
HBr leaching experiment (pH = 2.70, Eh = 705)	150 mL HBr + 150 mL distilled water	HBr-1	3.6	52.6	0.38	96.9	402	10.6	4.15	0.11
		HBr-2	1.02	23.8	0.17	27.5	182	4.76	6.62	0.17
		HBr-3	0.14	15	0.003	3.77	115	0.08	30.5	0.02
		HBr-4	0.1	15.1	0	2.69	115	0	42.8	0
		HBr-5	0.1	11.4	0.03	2.69	87.1	0.84	32.4	0.31
		Average	1	23.6	0.12	26.7	180	3.26	–	–
Oxalic acid leaching experiment (pH = 2.13, Eh = 453)	150 mL HCl + 50 g Oxalic acid + 150 mL distilled water	CS-1	4.84	83.5	3.16	130	638	88.5	4.91	0.68
		CS-2	46.6	167	15.7	1254	1276	440	1.02	0.35
		CS-3	42.6	125	27.2	1147	955	762	0.83	0.66
		CS-4	4.79	63.3	4.68	129	484	131	3.75	1.02
		CS-5	5.59	53.1	8.63	150	406	242	2.71	1.61
		Average	20.9	98.4	11.9	562	752	333	–	–
Citric acid leaching experiment (pH = 2.08, Eh = 475)	150 mL HCl + 50 g Citric acid + 150 mL distilled water	NMS-1	1.87	44.1	0.52	50.3	337	14.6	6.7	0.29
		NMS-2	4.15	64.9	0.58	112	496	16.2	4.43	0.14
		NMS-3	25	152	2.4	673	1162	67.2	1.73	0.1
		NMS-4	3.51	45.8	0.9	94.5	350	25.2	3.7	0.27
		NMS-5	2.98	32.7	0.96	80.2	250	26.9	3.12	0.34
		Average	7.5	67.9	1.07	202	519	30	–	–
Humic acid leaching experiment (pH = 2.86, Eh = 561)	150 mL HCl + 5 g Humic acid + 150 mL distilled water	FZS-1	4.03	54.8	1.83	108	419	51.3	3.88	0.48
		FZS-2	4	63.5	0.69	108	485	19.3	4.49	0.18
		FZS-3	7.77	75.6	2.36	209	578	66.1	2.77	0.32
		FZS-4	7.44	56.3	2.15	200	430	60.2	2.15	0.3
		FZS-5	12.9	83.5	7.05	347	638	198	1.84	0.57
		Average	7.23	66.7	2.82	194	510	79	–	–

Table 3
Concentrations of soaking solutions in laterite soaking experiments on the Lindai bauxite deposit.

Experiment name	Sample number	Reagent contents	Characteristic of solution	pH values	Eh (mV)	Al (ppm)	SiO_2 (ppm)	Fe (ppm)	K_{Al} (ug/g)	K_{Si} (ug/g)	K_{Fe} (ug/g)	K_{Si}/K_{Al}	K_{Fe}/K_{Al}
Ascorbic acid solution (strong reducing organic acid)	K-0	0.1 g	Have't adjust pH values	3.10	231	4.36	32.6	9.53	382	809	868	2.12	2.27
	K-1	0.2 g		2.92	233	5.78	37.6	16.9	506	934	1542	1.55	3.05
	K-2	0.5 g		2.73	222	8.27	42.7	28.2	724	1061	2566	1.47	3.54
	K-3	0.5 g	Add 0.5 g Ascorbic acid, use HCl and	3.00	203	7.37	36.3	22	645	901	2006	1.4	3.11
	K-4	0.5 g	NaOH solution to adjust pH to	4.99	73	3.17	17.2	5.05	278	427	460	1.54	1.65
	K-5	0.5 g	specified values	7.02	−9	2.07	13.5	1.49	181	335	135	1.85	0.75
	K-6	0.5 g		8.99	−20	2.06	12.7	1.2	175	316	109	1.76	0.61
Nitric acid solution (oxidizing inorganic acid)	N-1	0.5 ml	Add 0.5 mL HNO_3, use HCl and	3.02	435	0.33	11.6	0.56	29.2	287	51.4	9.9	1.76
	N-2	0.5 ml	NaOH solution to adjust pH to	5.03	328	0.12	5.69	0.18	10.7	141	16.7	12.8	1.55
	N-3	0.5 mL	specified values	7.01	269	0.16	3.88	0.32	14.4	96.4	29.5	6.86	2.14
	N-4	0.5 mL		9.01	255	0.11	2.36	0.13	9.24	58.7	11.6	6.56	1.33
Hydrobromic acid solution (weak reducing inorganic acid)	X-1	0.5 mL	Add 0.5 mL HBr, use HCl and NaOH	3.00	424	0.12	9.96	0.15	10.3	247	13.5	24	1.31
	X-2	0.5 mL	solution to adjust pH to specified	4.98	320	0.17	7.09	0.17	14.5	176	15	11.7	1.03
	X-3	0.5 mL	values	7.03	254	0.1	3.62	0.03	8.55	90	3.06	10.5	0.33
	X-4	0.5 mL		9.00	221	0.15	2.7	0.17	12.8	67	15.9	5.15	1.23
Humic acid solution (mixed organic acid)	F-2	0.1 g	Add 0.5 g Humic acid, use HCl and	3.00	405	2.4	20.2	0.98	210	502	89.7	2.39	0.43
	F-3	0.1 g	NaOH solution to adjust pH to	5.02	320	5.01	13	2.33	439	322	212	0.73	0.48
	F-4	0.1 g	specified values	7.00	283	4.63	7.04	2.15	405	175	196	0.43	0.48
	F-5	0.1 g		9.00	256	3.72	3.56	2.19	326	88.4	199	0.27	0.61

Table 4
Relative abundance (wt.%) of minerals in selected bauxite samples from XRD.

Sample No.	Lithology	Major minerals (wt.% > 15%)	Minor minerals (wt.% < 15%)
LD-2	Compact bauxite	Boehmite, Kaolinite	Illite, Smectite, Quartz, Dolomite, Anatase, Rutile
LD-3	Ferruginous clay	Kaolinite	Illite, Smectite, Quartz, Boehmite
LD-4	Bauxite clay	Boehmite, Kaolinite, Illite	Smectite, Quartz, Dolomite
LD-7	Clastic bauxite	Diaspore	Dolomite, Goethite, Anatase, Rutile
LD-8	Bauxite clay	Kaolinite, Boehmite	Quartz, Goethite, Feldspar
LD-10	High-iron bauxite	Diaspore, Hematite	Quartz, Smectite, Anatase
LD-11	Loose laterite	Quartz, Illite, Hematite, Dolomite	Kaolinite, Smectite
LD-12	Massive laterite	Quartz, Illite, Hematite, Dolomite	Kaolinite, Smectite

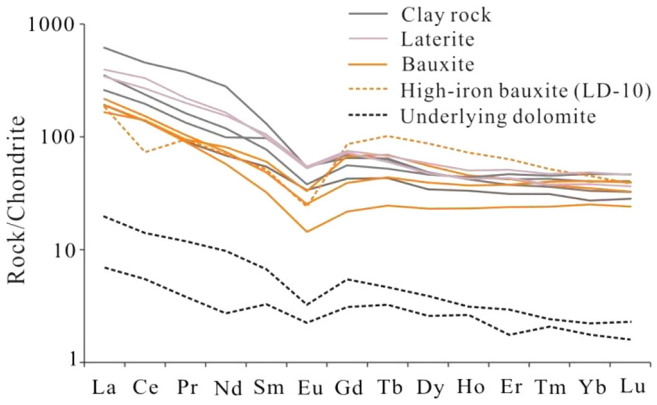

Fig. 6. Chondrite-normalized REE patterns of samples from the Lindai bauxite deposit (normalized values from Sun and McDonough, 1989) showing that the basement dolomites, Al-bearing rocks, and laterites display similar REE patterns.

acids, HCl provides the most conducive environment for element migration, although it is not as good as the organic acids (Fig. 7a and b). Overally, the rate of Si migration is higher than Fe and Al in both organic and inorganic conditions. The Si and Al concentrations observed in presence of humic acid conditions are lower than those in citric acid conditions, in contrast to the Fe concentration. This result from the significant amount of humilic acid contained in humic acid; humilic acid is insoluble in acidic solution and inhibits the migration of the three elements (it could be seen that the humic acid did not dissolve completely during the experiment). However, with the exception of oxalic acid, the Fe concentration in presence of humic acid conditions is higher than that in the other conditions due to the presence of a reducing acid in the humic acid condition. The Si/Al and K_{Si}/K_{Al} values are higher than 1 in all conditions (Fig. 8), indicating that Si removal and Al enrichment occur easily under all conditions. Particularly in weak reducing HBr conditions, Si/Al values reach 100 and even more, and K_{Si}/K_{Al} values exceed 30 (Fig. 8a and b; Table 2), indicating that this reducing inorganic acid favors Si leaching. However, the Fe/Al and K_{Fe}/K_{Al} values are different from the Si/Al and K_{Si}/K_{Al} values (Fig. 8c and d), which are lower than 1 in all conditions except in the late stage of oxalic acid conditions (1.54 and 1.61, respectively) (Table 2). This indicates that Fe is more difficult to leach than Si and Al; Fe removal and Al enrichment are possible only under suitable reducing organic acid conditions. Fe/Al and K_{Fe}/K_{Al} values are higher in the first sampling than in the second sampling, which might result from the leaching of more free-form Fe from the sample or the flushing effect on sample columns by solution leaching in the early experimental stages (Fig. 8c and d). The reliability of the above results is demonstrated by the similar pH values of "rainwater" (between 2 and 3) in all experiments (Table 2).

4.4.2. Soaking experiments

The concentrations and migration rates of Al, Si, and Fe are negatively correlated with pH values, except in presence of humic acid conditions (Fig. 9). Thus, acidic conditions are more favorable to the migration of these three elements than neutral and alkaline conditions. The different result obtained in case of humic acid results from its low solubility in acidic solutions; this also explains why Fe and Al concentrations at pH = 3 are lower than those at other pH values (Fig. 9f). At the same pH value, Si concentrations are higher than the other two elements, implying that Si can be removed easily, whereas Fe and Al are difficult to migrate. Particularly in inorganic acid conditions, Si concentrations (2.36–11.6 ppm) are much higher (even more than 50 times higher) than those of Fe and Al (0.03–0.56 ppm; Fig. 9a and b).

Table 5
Selected elements and ion concentrations in pit water and affected surface water from the Jiuan and Xingren coal mines (Xinren-1, 2 from Wu et al., 2009).

Sample number	Sampling date	pH	Total iron (mg/L)	Fe^{2+} (mg/L)	SO_4^{2-} (mg/L)	Al (ppm)	Si (ppm)	Ca (ppm)	Mg (ppm)
Jiuan-1	2012.10	2.98	1348	–	5887	298	186	528	271
Jiuan-2	2013.9	2.81	1304	1258	6646	–	–	–	–
Jiuan-3	2013.9	2.81	1273	971	6838	–	–	–	–
Xinren-1	2005.4	3.02	109	–	2275	104	–	362	116
Xinren-2	2005.4	2.69	742	–	3483	180	–	326	75.4

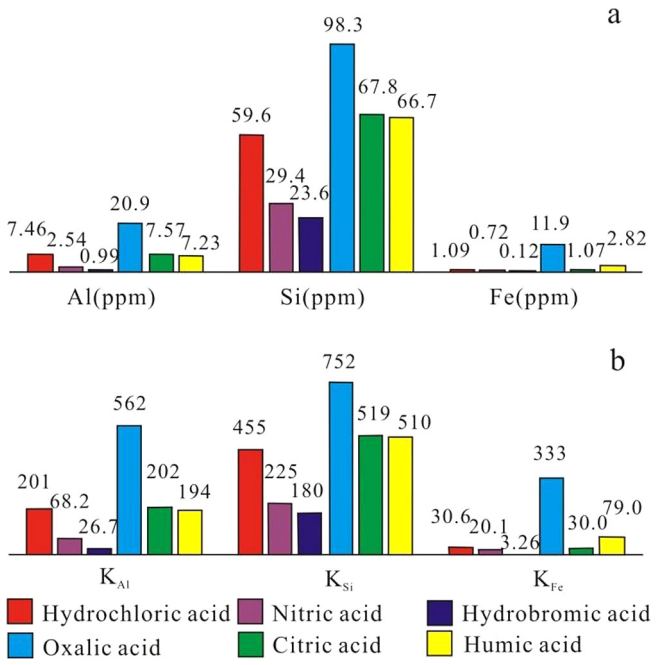

Fig. 7. Diagrams showing the concentrations of Al, Si, Fe (a) and K_{Al}, K_{Si}, K_{Fe} values (b) for massive laterite leaching experiments with different acids.

Moreover, the concentrations of these three elements in organic acid solutions are much higher than those in inorganic acid solutions (Fig. 9). Organic acids apparently favor the migration of these three elements more than inorganic acids. In organic acid experiments (Fig. 9c and d), the concentrations of these three elements at pH = 3 (strong acidic conditions) are much higher than those at the other three pH values. In nonreducing organic acid conditions (Fig. 9e and f), moderate improvements in the migration of the three elements at different pH values were observed; the concentrations of the three elements in nonreducing organic acid solutions (at pH = 5, 7, and 9) are higher than those in reducing organic acid solutions (Fig. 9c, d and e). Similar to the leaching experiments, the low solubility of humic acid results in lower Fe and Al concentrations in the humic acid soaking experiments at pH = 3 compared to the other three pH values; the Si concentration is highest at pH = 3 (Fig. 9f).

In most cases, K_{Si}/K_{Al} values are higher than K_{Fe}/K_{Al} values, implying that Si removal is easy compared to Fe, in agreement with the results of the leaching experiments (Fig. 10). In soaking experiments with different concentrations of ascorbic acid (0.1, 0.2 and 0.5 g), K_{Fe}/K_{Al} values improve from 2.27 to 3.55 with the addition of ascorbic acid, while K_{Si}/K_{Al} values show the reverse trend (Fig. 10e; Table 3). Fig. 10f shows a similar situation; as pH values increase, K_{Fe}/K_{Al} values decline, while K_{Si}/K_{Al} values increase slightly. These results indicate that lower pH values and higher concentrations of ascorbic acid favor Fe removal and Al enrichment. When 0.5 g ascorbic acid is added to 50 ml water, the solution pH is 2.73 (Fig. 10e; Table 3); on increasing the pH to 3.00 (Fig. 10f), the values of K_{Fe}/K_{Al} and K_{Si}/K_{Al} decrease from 3.55 to 3.11 and from 1.47 to 1.40, respectively (Table 3). This indicates more acidic solutions result in the easier removal and enrichment of Fe and Al, respectively (especially the Fe removal). The K_{Si}/K_{Al} values are higher than 1 in the three inorganic acid conditions, but generally lower than 1 in organic acid conditions (Fig. 11a). This indicates that Si migrates easily in natural conditions; any type of inorganic acid and any pH value favor Si migration. K_{Fe}/K_{Al} values, however,

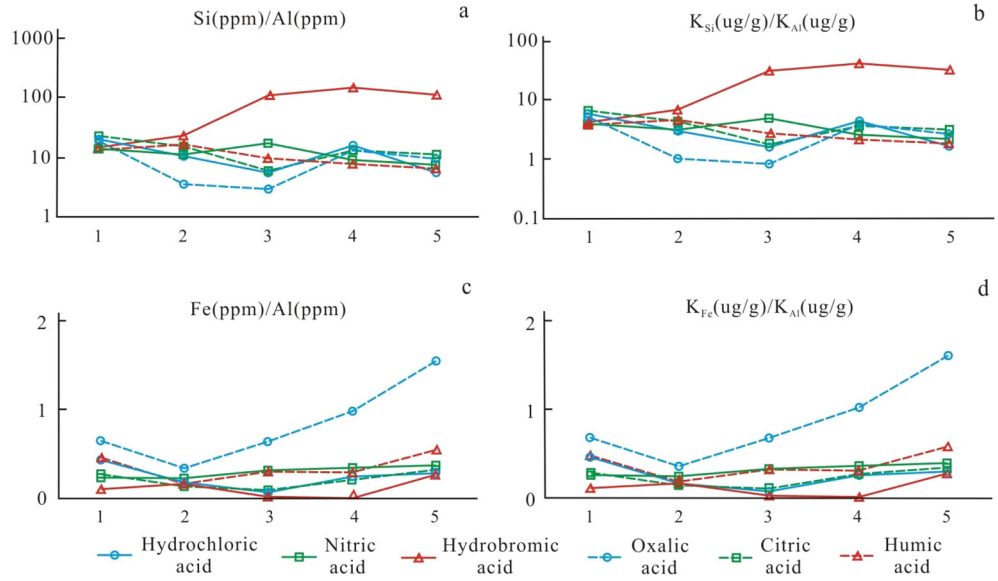

Fig. 8. Diagrams showing the values of Si/Al (a), K_{Si}/K_{Al} (b), Fe/Al (c), and K_{Fe}/K_{Al} (d) for massive laterite leaching experiments with different acids. Abscissa axis means times of sampling, the units of vertical axis are "1".

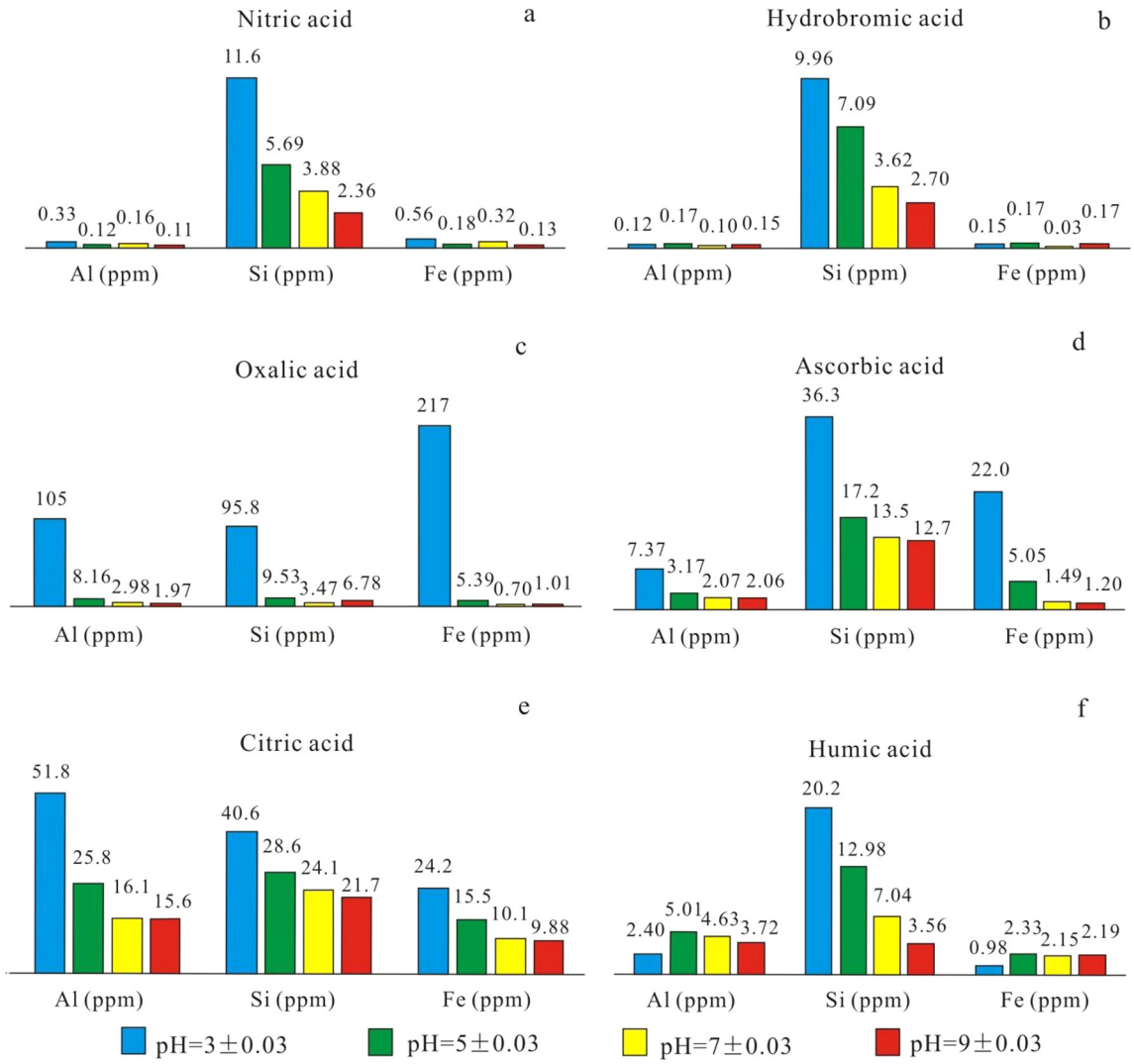

Fig. 9. Diagrams showing the concentrations of Al, Si, Fe for massive laterite soaking experiments with nitric acid (a), hydrobromic acid (b), oxalic acid (c), ascorbic acid (d), citric acid (e), and humic acid (f). The oxalic and citric acid data are from Ling et al. (2013).

exceed 1 only in oxalic acid (at pH = 3) and ascorbic acid (at pH = 3 and 5) conditions (2.14, 3.11, and 1.65, respectively; Fig. 11b). Thus, Fe migration is difficult in natural conditions; Fe removal and Al enrichment can be achieved only in strong acid and reducing organic acid conditions. The K_{Si}/K_{Al} values in HNO_3 and HBr conditions are also higher than 1, but the Fe concentrations in these conditions (0.03–0.56 ppm) are much less than those in oxalic and ascorbic acid conditions (5.05–217 ppm; Fig. 11a and b); therefore, HNO_3 and HBr have limited effects on Fe removal and Al enrichment. Strong acidic and reducing organic conditions were apparently highly favorable for Fe removal and Al enrichment during the metallogenic period of karstic bauxite deposits.

5. Discussions

5.1. Elemental behaviors and precursor rocks of bauxite

5.1.1. Elemental behaviors

The chemical indices of alteration ($CIA = Al_2O_3/(Al_2O_3 + CaO + Na_2O + K_2O) \times 100$) (Nesbitt and Yong, 1982) of those four bauxite samples (LD-2, 7, 9 and10) are higher than 96, indicating that these samples experienced complete weathering. While two laterite samples have lowest CIA values (average 73), suggesting that they did not experience complete weathering; bauxite clay and clay samples have middle CIA values (on average 93.7) (Table 1). TiO_2 and Zr contents are positively correlated with Al_2O_3 content, with R values of 0.90 and 0.92, respectively (Fig. 12a and b); this implies that Al also acts as a conservative element during weathering processes.

As mentioned in the previous section, the average ∑REE of laterite, clay, and bauxite samples are 434.5, 382.2, and 216.6 ppm, respectively. The laterite and clay samples have higher ∑REEs than bauxite samples, which is explained by the difference in REE adsorption by clay minerals. The absorption energy of an REE^{3+} is related to its ionic radius and increases with decreasing ion size in ascending order from La–Ce to Yb–Lu (Ye et al., 2007; Ling et al., 2013). Therefore, laterite and clay samples that are enriched with clay minerals have high contents of ∑REE and LREE along with higher LREE/HREE values (Tables 1 and 4). Variations of La/Y ratios in bauxites are suitable parameter for determination of pH during bauxite formation (Crnicki and Jurkovic, 1990; Maksimovic and Panto, 1991; Zarasvandi et al., 2012; Zamanian et al., 2016; Radusinović et al., 2017). La/Y >1 indicate alkaline conditions, whereas La/Y <1 indicate acidic conditions. In the Lindai bauxite, La/Y ratios in the bauxitic clay and clay samples are mostly greater than 1 and those ratios in the high-quality bauxites (LD-7, 10) show lowest La/Y values, i.e., 0.55 and 0.38, respectively

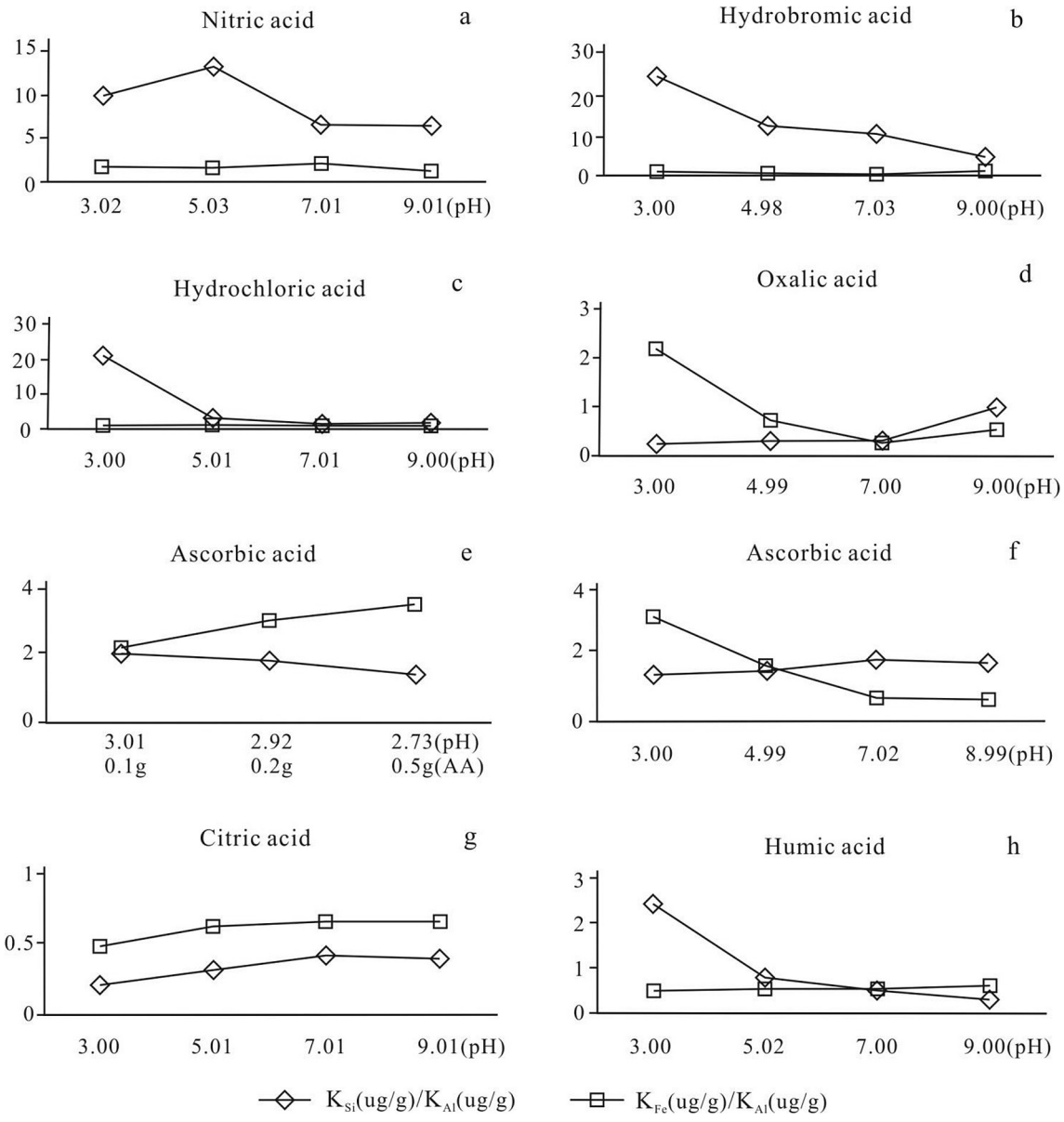

Fig. 10. Diagrams showing the values of K_{Si}/K_{Al} and K_{Fe}/K_{Al} for massive laterite soaking experiments with nitric acid (a), hydrobromic acid (b), hydrochloric acid (c), oxalic acid (d), ascorbic acid (e, f), citric acid (g), and humic acid (h). Figure e is different from the others because the pH was not adjusted by HCl and NaOH solutions (AA represents ascorbic acid). The hydrochloric, oxalic, and citric acid data are from Ling et al. (2013). The units of vertical axis are "1".

(Table 1), indicating that high-quality bauxites are formed under acidic hydrogeological condition during the ore–forming process in the Lindai district.

As mentioned above, most of the samples show medium and positive Ce anomalies (i.e., average 1.03) with the exception of sample LD-10 (high-iron bauxite with Ce depletion, $Ce/Ce^* = 0.55$) in the Lindai profile (Table 1; Fig. 6). There is a strong relationship between REE ionic potential and their mobility (Esmaeily et al., 2010). Under acidic and oxidizing conditions, LREEs can be easily leached from the upper parts and concentrated in the lower section due to the lower ionic potential of LREE compared to HREE (Esmaeily et al., 2010; Mongelli et al., 2014; Zamanian et al., 2016). However, Ce exists naturally in two forms (i.e., Ce^{3+} and Ce^{4+}), and the Ce^{4+} has a higher ionic potential relative to the other LREE, consequently, Ce is usually retained in the upper parts of the weathering profiles due to the oxidation of Ce^{3+} to Ce^{4+} (Esmaeily et al., 2010; Karadağ et al., 2009; Mongelli et al., 2014; Zamanian et al., 2016). On the contrary, under reducing conditions, Ce^{4+} would reduction into Ce^{3+} which shows higher mobility (Wang et al., 2010; Li et al., 2013). Therefore, Ce mainly exists in the Ce^{3+} form and significant migration of Ce^{3+} results in Ce depletion in the high-iron bauxite (LD-10; Fig. 6). The existence of siderite and pyrite (Fig. 3c) in LD-10 also indicates that it was formed under reducing conditions.

5.1.2. Precursor rocks of bauxite

Even though the source rocks of karstic bauxites have been investigated for decades using trace element signatures (Özlü, 1983; Karadag et al., 2009; Wang et al., 2010; Zarasvandi et al., 2010; Zamanian et al., 2016), detrital mineral characteristics (D'Argenio and Mindszenty, 1995; Mordberg et al., 2000), and U-Pb ages of detrital zircons (Deng et al., 2010; Boni et al., 2012; Gu et al., 2013b; Cai et al., 2015; Wang et al., 2016), the source rocks of the karstic bauxite deposits remain controversial. In the Xiuwen bauxite ore belt, based on the geological survey and the geochemical studies of ores, most researchers have suggested that the underlying Middle and Upper Cambrian dolomite is the precur-

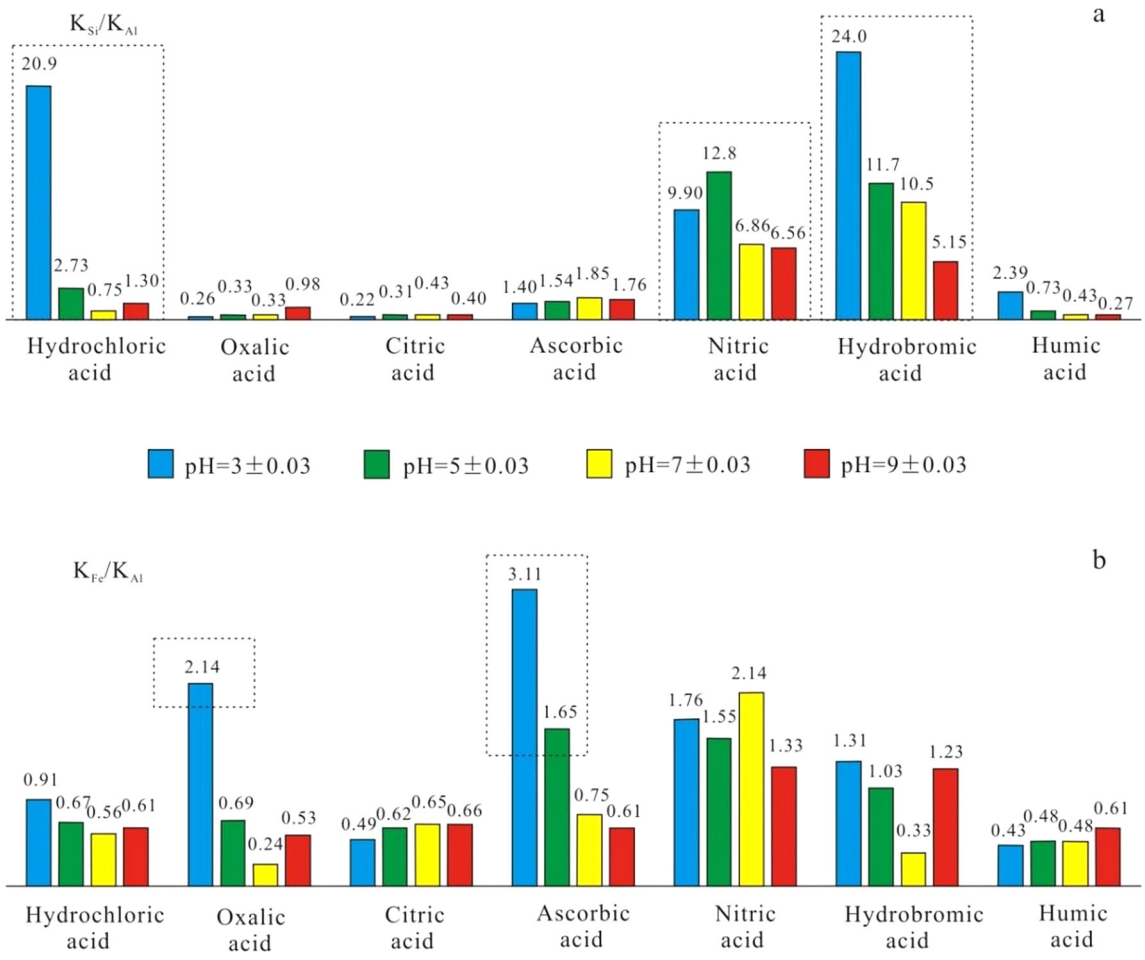

Fig. 11. Diagrams showing the values of K_{Si}/K_{Al} (a) and K_{Fe}/K_{Al} (b) for massive laterite soaking experiments (the hydrochloric, oxalic, and citric acid data are from Ling et al., 2013).

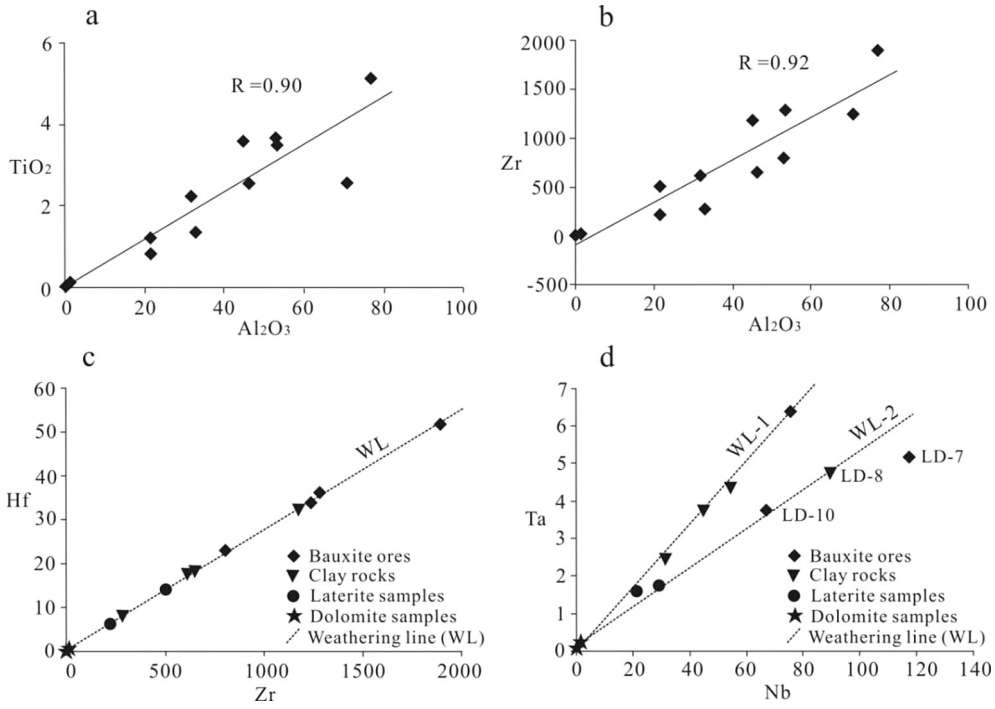

Fig. 12. Bivariate plots of (a) Al_2O_3 vs. TiO_2, (b) Al_2O_3 vs. Zr, (c) Zr vs. Hf, and (d) Nb vs. Ta.

sor rock of the bauxite (Bárdossy, 1982; Gao et al., 1992; Ye et al., 2007; Ling et al., 2013).

The MgO contents (average 4.23 wt.%) of the two modern weathered laterite samples of the Middle Cambrian Shilengshui Formation dolomite are higher than their CaO contents (average 1.65 wt.%) (Table 1). It is explained by the fact that Ca is more chemically active than Mg in the weathering and deposition processes (Ji et al., 2004). The observed MgO contents of all ore-bearing rock samples range from 0.16 wt.% to 0.68 wt.%, while the CaO content could only be detected in a single sample (LD-1, 0.06 wt.%) (Table 1). The XRD results revealed that dolomites are widespread in ore-bearing rock series such as LD-2, LD-4, and LD-7 (Table 4). The occurrence of dolomite and high contents of MgO may be evidence that the underlying dolomites are the precursor rocks of the ore-bearing rock series.

Previous studies suggested that the Eu anomaly is retained during intense weathering (Mongelli, 1997; Mameli et al., 2007). Therefore, Eu/Eu* index were used for determination of precursor of bauxites (Liu et al., 2010; Wang et al., 2010; Abedini and Calagari, 2013). The similarity of Eu/Eu* values in the dolomites (0.71 and 0.53, average 0.62), laterites (0.59 and 0.62, average 0.61), and ore-bearing rocks (0.52–0.7, average 0.59; with the exception of high-iron bauxite, i.e., LD-10) indicate that parent rocks shared by the bauxites and laterites might be the dolomites (Table 1). The ratios of immobile elements (e.g., Zr/Hf, Nb/Ta, and Y/Ho) in bauxite are considered to be similar to those of the parent rocks and can be used to determine source rocks (Valeton et al., 1987; MacLean et al., 1997; Calagari and Abedini, 2007; Liu et al., 2010; Zamanian et al., 2016). When plotted in cross-plots, these ratios create linear arrays with high correlations that pass through the data point belonging to the parent rock(s) (MacLean, 1990). As mentioned in previous section, the similar Y/Ho and Zr/Hf ratios between dolomites and ore-bearing rocks indicate that the two types of samples are genetically related. In addition, the plots of the dolomites and laterites lie almost on or close to the weathering line fit by the Al-bearing rocks in Zr vs. Hf and Nb vs. Ta diagrams (Fig. 12c and d). This also suggests that there is an intimate genetic correlation between the Lindai bauxite deposits and the underlying dolomite. The two sampling sites separated by one kilometer result in the existence of two weathering lines (i.e., WL-1 and WL-2) in the Nb/Ta diagram. Different formation environments (i.e., wind, sunshine, and hydrogeochemical conditions, etc.) between the open pit and profile samples caused the different Nb/Ta ratios and weathering lines.

REE patterns can also be used to identify source materials (Esmaeily et al., 2010; Wang et al., 2010). As already reported, the REE patterns of the Lindai bauxite and laterite samples are similar to those of the underlying dolomite; LREEs and HREEs are strongly enriched in the bauxite deposits compared to the dolomite (Fig. 6). In addition, the bauxite ores and the underlying dolomite show similar Eu negative anomalies (Fig. 6). Therefore, the similarities in the REE patterns and Eu anomalies of bauxites, laterites, and underlying dolomites imply that the dolomites are the parent rocks of these weathering products. The above discussion indicates that source rocks shared by the bauxites and laterites might be the underlying Shilengshui Formation dolomites. The weathered laterite was produced during the conversion of precursor rocks to bauxite.

5.2. Discussion of the key issues regarding simulated weathering experiments

At the beginning of the simulated weathering experiments, Al, Si, and Fe (present in their free states) might be removed. Kaolinite, illite, and other clay minerals were partially hydrolyzed, and metal cations were extracted by the leaching solutions. Silicon mainly existed as silicon dioxides or silicate minerals. However, silicon dioxides are extremely stable in a supergene environment; thus, the Si in carbonates mainly originated from the decomposition of silicate minerals (White et al., 1996). Iron and alumina mainly existed in the forms of ions, hydroxides, or organic complexes, whereas Si existed in the form of SiO_2, metasilicic acid (H_2SiO_3), or orthosilicic acid (H_4SiO_4) in experimental solutions as well as in natural environments (White et al., 1996).

Taken into account Figs. 7–11 and foregoing related arguments, the leaching and soaking experiments result in the similar conclusions: (1) Si is easily migrated in most conditions, especially in acidic and reducing inorganic solutions, and (2) the migration of Fe is difficult; only in an acidic and reducing condition with presence of organic materials are removal of Fe and Al enrichment are possible. Whether the reducing condition or the presence of organic materials induces Fe removal, however, is not clear. In the leaching experiments, the Fe concentrations in HCl and HNO_3 solutions are 1.09 and 0.72, respectively, whereas those in oxalic acid, citric acid, and humic acid conditions are 11.9, 1.07, and 2.82, respectively. These concentrations indicate that the reducing acid (i.e., oxalic acid) had the greatest effect on Fe removal; nonreducing or weak reducing organic acids (i.e., citric and humic acids) had trivial effects on Fe migration (Fig. 7a and b), implying that a reducing condition is important for Fe removal. However, the weak reducing inorganic acid solution of HBr resulted in the lowest concentration of Fe, even lower than that in HCl and HNO_3 conditions (Fig. 7a and b). This indicates that the presence of organic compounds is also important for Fe removal. Similar results were observed in the soaking experiments; at pH = 3, the level of Fe migration in oxalic acid conditions was higher than those in citric, humic, and HBr acid conditions (Fig. 9b–f). Based on the discussion above, it can be concluded that acidic conditions, reducing conditions, and organic materials are essential factors that can play a great role in high-quality karstic bauxite formation during sedimentation–diagenesis processes. Reducing and acidic diagenetic environments for karstic bauxites had also been reported in previous studies (Özlü, 1983; D'Argenio and Mindszenty, 1995; Temur and Kansun, 2006; Liu et al., 2010; Wang et al., 2011a; Laskou and Economou-Eliopoulos, 2013).

5.3. Compatibility of the experimental results with the geological characteristics

5.3.1. Migration of Fe and Si during the metallogenic period of karstic bauxite

Lateritic bauxite mainly consists of Al_2O_3 (40–60%), SiO_2 (2–20%), and Fe_2O_3 (10–30%) (Bárdossy, 1982; D'Argenio and Mindszenty, 1995). High-quality karstic bauxites, however, have higher Al_2O_3 contents (more than 70 wt.%; e.g., LD-7 and LD-10), lower Fe_2O_3 contents (less than 3 wt.%; e.g., LD-2, LD-4, LD-7, and LD-8), and lower SiO_2 contents (e.g., LD-7 and LD-10). Therefore, the conversion of lateritic bauxite into karstic bauxite requires Si and Fe removal and Al retainment (Patterson, 1967; Laskou and Economou-Eliopoulos, 2007, 2013; Mameli et al., 2007). This requires suitable hydrogeological conditions since lateritic bauxite or Al-rich laterite deposited in karst depressions or basins, which shows the importance of the hydrogeological conditions. These facts are completely consistent with the aim of the simulated weathering experiments in this study, which is to simulate the most suitable hydrogeological conditions during karstic bauxite mineralization.

5.3.2. The "coal–bauxite–iron" structure

The "coal–bauxite–iron" structure had been discovered in many bauxite deposits around the world, including the central Guizhou bauxites ore field (Clarke, 1966; Demina, 1977; Bárdossy, 1982; Calagari and Abedini, 2007; Kalaitzidis et al., 2010; Zhang et al., 2013). Extensive development of plants during the Carboniferous

provided rich organic material for the formation of the coal layers overlying the initial bauxitic materials (Du and Tong, 1998). Pyrite and other sulfides in coal were easily oxidized to produce acidic and reducing groundwater with organic materials (H_2S, H_2SO_4, etc.) that percolated downward, resulting in the bleaching and Al enrichment of the upper part of the underlying bauxites (Kalaitzidis et al., 2010). This groundwater also reduced Fe^{3+} to the easily migrating form Fe^{2+} and transported it down close to the carbonate basement to precipitate iron (FeS_2, $FeCO_3$, etc.) in the "coal–bauxite–iron" structure (Mameli et al., 2007; Kalaitzidis et al., 2010; Ling et al., 2013; Zhang et al., 2013).

Coal layers are typically oxidized to form acidic and reducing groundwater (Patterson, 1967; Kalaitzidis et al., 2010; Ling et al., 2013). As reported before, the pit water from the Jiuan coal mine tunnel with a high total iron concentration was strongly acidic, and the iron migrating in the pit water was mainly in the form of Fe^{2+}. To verify the accuracy of the pit water analysis, the affected surface water of the Xingren coalfield, Guizhou Province was quoted (Wu et al., 2009); it showed similar geochemical characteristics: low pH values (2.69–3.02) and high concentrations of Fe (109–742 ppm), SO_4^{2+} (2275–3483 ppm), and Al (104–180 ppm) (Table 5). The high concentration of iron in the pit water and affected surface water are due to their leaching from the coal layers and wall rocks by the acidic and reducing groundwater (Kalaitzidis et al., 2010; Laskou and Economou-Eliopoulos, 2013). Iron concentrations were higher than those of Al in the pit water and affected surface water, similar to the results of the oxalic and ascorbic acid soaking experiments (characteristics by acidic and reducing conditions with organic materials) (Fig. 9c and d, pH = 3). Pit water, affected surface water, oxalic, and ascorbic acid solutions appear to favor Fe migration, which are consistent with our experimental results, indicate that the acidic and reducing groundwater with organic materials derived from the upper coal layers result in bauxite mineralization. In addition, oxalic and ascorbic acids are widely distributed in nature; it is present in almost all plants. Dead plants release a large amount of organic matter such as oxalic and ascorbic acids, which leache the underlying bauxitic material to form high-quality bauxite (Patterson, 1967; Kalaitzidis et al., 2010; Laskou and Economou-Eliopoulos, 2007, 2013).

5.3.3. Effects of organic matter on Si and Fe migration

Available information indicates that the complex making abilities of dissolved organic matters with heavy metal ions are related to molecular groups (such as carboxyl groups and amino group), and particularly related to undissociated carboxyl contents (Kuiters and Mulder, 1992; Han and Thompson, 1999). Different metal ions with different electronic shells have varying abilities to accept electron pairs. Therefore, the complexation ability of organic matter varies is based on the metal ion; in general, $Fe^{2+} > Al^{3+}$. In this regard, Si^{4+} is the weakest because of its existence in water in the forms of H_4SiO_4 and H_2SiO_3, which form weak complexes with organic matter (Kuiters and Mulder, 1992; Han and Thompson, 1999). Öztürk et al. (2002) investigated the Dogankuzu and Mortas bauxite deposits in Taurides and presented the same opinion: carbon and sulfur isotope compositions emphasize the importance of organic matter and bacterial processes during deposition and mineralization. These findings are coincided well with the experimental results suggesting that organic conditions strongly promote migrations of Al, Si, and especially that of Fe. Active groups such as carboxyl and hydroxyl groups in organic acids (e.g. oxalic acid, humic acid), act an important roles during the mineralization of karstic bauxites and supergene processes. The promotion of element migration by organic matter may be explained as follows: (1) organic matter can promote the proton implantation of minerals, accelerating mineral hydrolysis and causing structural damage to extract metal cations; (2) organic matter can form complexes with metals, enhancing the dissolution of these three elements; (3) organic matter can create reducing conditions that strongly promote Fe migration (Leanard, 1982; Chen, 1991, 1996).

5.4. Importance of hydrogeological conditions during formation of karstic bauxite

Diagenetic environments and hydrogeological conditions of karstic bauxites have been involved in previous studies (Grubb, 1970; Özlü, 1983; D'Argenio and Mindszenty, 1995; Temur and Kansun, 2006; Liu et al., 2010; Wang et al., 2011a; Laskou and Economou-Eliopoulos, 2013). For instances, Liu et al. (2010) investigated the Dajia bauxite deposit in Western Guangxi, China. They suggested that the depositional/diagenetic environments and hydrogeological conditions of the bauxite were closer to phreatic environments with dominant reducing conditions. Moreover, the environment of the bauxite deposit during a metadiagenetic stage was chemically reducing due to the decomposition of organic material and acidic due to the decomposition of pyrite (Laskou and Economou-Eliopoulos, 2013, and references therein). The presence of sulfides in ores of the Dogankuzu and Mortas bauxite deposits in Taurides, Turkey indicates that the early diagenetic environment of the bauxite was reducing (Öztürk et al., 2002). In general, the hydrogeochemistry and geochemistry for the depositional/diagenetic environments of bauxite formation can be characterized as "vadose type" (high-level karst terrain) and "phreatic type" (low-level karst terrain) (Combes, 1969; Komlóssy, 1970; Valeton, 1972; Bárdossy, 1982; D'Argenio and Mindszenty, 1995; Liu et al., 2010; Wang et al., 2011a; Zamanian et al., 2016). The vadose-type bauxites have a high groundwater table; thus, the unobstructed drainage and neutral or oxidizing conditions are characterized by gibbsite, boehmite, hematite, and goethite (Bárdossy, 1982; D'Argenio and Mindszenty, 1995; Liu et al., 2010). In contrast, the phreatic bauxites often have a low groundwater table, stagnant groundwater, and reducing conditions, resulting in diaspore and boehmite as aluminum-rich minerals and goethite, siderite, and pyrite as iron minerals (Bárdossy, 1982; D'Argenio and Mindszenty, 1995; Liu et al., 2010). So, it is indicated that the geochemistry of the depositional/diagenetic environments of the Lindai karstic bauxite were reducing and acidic due to its phreatic type mineral assemblage of diaspore + siderite + pyrite.

The diagenetic environments and hydrogeological conditions are important for mineralization of karstic bauxite deposits, since Si and Fe removal and Al enrichment are the essential processes for karstic bauxite formation (Patterson, 1967; Laskou and Economou-Eliopoulos, 2007, 2013; Mameli et al., 2007). It requires a suitable hydrogeological condition to transform lateritic bauxite or Al-rich laterite into karst depressions/basins. Consequently, above discussions and our simulated weathering experiments reveals that the acidic, reducing, and organic materials occurrences are essential hydrogeological conditions for high-quality karstic bauxite mineralization.

6. Metallogenic model

Based on our simulated weathering experiments and previous studies, the metallogenic model of the karstic bauxite deposit belts in Central Guizhou Province can be summarized as follows (Fig. 13):

(1) Due to the Early Paleozoic Caledonian movement, central and north Guizhou were uplifted to land (Guizhou Provincial Bureau of Geology and Mineral Resources, 1987). It was followed by the processes of denudation and peneplanation over almost 100 Ma, causing the Devonian,

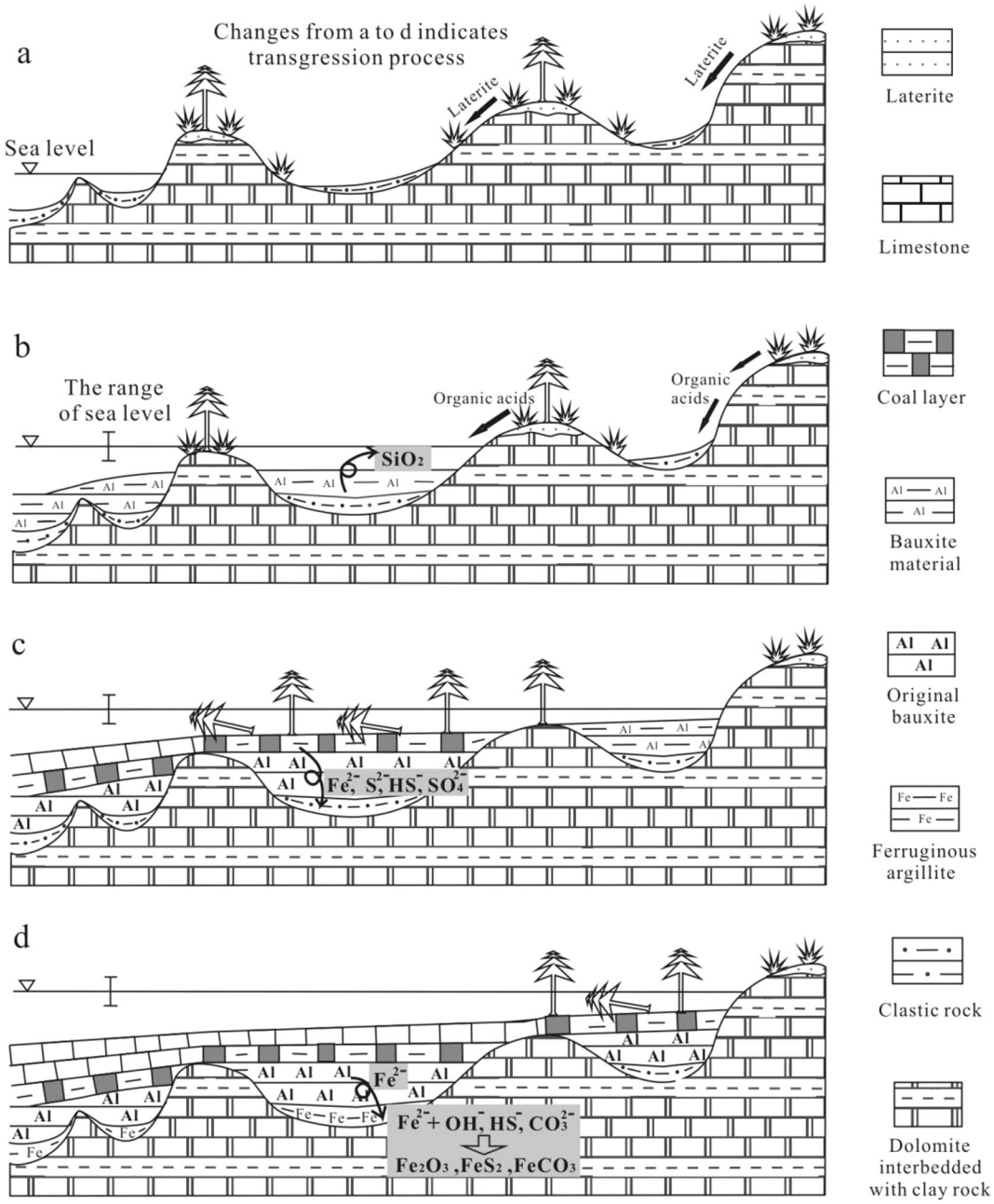

Fig. 13. Schematic geological cross-section of the Central Guizhou Province, SW China, illustrating the metallogenic model of the karstic bauxite deposits in Central Guizhou Province. (a) The South China Sea transgressed with sea-level changes (10–120 m) in the Early Carboniferous (Joachimski et al., 2006); (b) the original bauxitic material (lateritic bauxite or Al-rich laterite) was then transported from land to karst depressions/basins by surface water. The SiO_2 were migrated through neutral to acidic and/or weak reducing water derived from extensive vegetation development (forming organic acid) in semi-closed karst depressions and lands; (c) abundant organic matter, overlying bauxitic material, formed coal layers, which could produce acidic and reducing groundwater (S^{2-}, HS^{-}, SO_4^{2-}, etc.) with organic materials via oxidization. During transgressive cycles (especially in sea-level declined), the groundwater leached downward and extracted Fe from bauxitic material, resulting in the high quality bauxites; (d) and the Fe ions migrated downward to basal carbonate, and precipitated under alkaline conditions to develop ferruginous rocks (Fe_2O_3, FeS_2, $FeCO_3$, etc.). During the Late Triassic, tectonic movement uplifted the initial bauxite and clay bauxite to near the surface. The coal beds or carbonaceous shales continued to produce the acidic and reducing groundwater and cause secondary alteration and the enrichment of the initial bauxite and clay bauxite, ultimately forming the high-quality bauxite that is available for industrial exploitation.

Silurian, and Ordovician strata absent in central Guizhou and formed a quasi-lysogenic landform including several karst depressions and basins that were favorable places for bauxite deposition (Gao et al., 1992). According to the paleomagnetic remanence analysis, Guizhou was located at 8–14° south latitude in the Carboniferous (Liu et al., 1990), had a hot and humid tropical climate, and was conducive to the formation of a laterite weathering crust; thus, it was able to provide the necessary climatic conditions for the formation of the bauxite deposits. Impure dolomites or interbedded clay rocks of the Middle Cambrian Shilengshui Formation experienced intense weathering in the tropical humid climate. K, Na, Ca, Mg, and other active elements were migrated out, while Fe, Al, Ti, Si, and other relatively inactive elements remained in the paleo-weathering crust to form lateritic bauxite or Al-rich laterite (Fig. 13a).

(2) During the Carboniferous, the transgression of the South China Sea from south to north led to the deposition of lateritic bauxite or Al-rich laterite derbis in karst depressions or catchment basins, forming the initial bauxitic material

(mainly consisting of gibbsite and clay minerals). The Lindai bauxite was formed by paleo-laterites deposited in the "Xiuwen, Qingzhen karst basin" (Gao et al., 1992). A transgression process, however, does not indicate a continuous sea level increase; instead, changes in sea level often occur because of many transgression cycles (sea level rising and falling). Joachimski et al. (2006) suggested that changes in global sea level in the Carboniferous–Permian may reach 10–120 m. The rising and falling of the sea level led to good drainage conditions in the bauxitic material sedimentary area which favoring karst bauxite formation (Wang et al., 2011b). Especially, when sea level falls, Fe is removed down to near the basal carbonates to precipitate the iron rocks under oxidation environment. At the same time, plants began to spread across lands during Devonian and Carboniferous eras, and Chinese flora prospered in the Permian period (Du and Tong, 1998). Hot and humid tropic climate contributed to the flourishing of plants, and dead plants produced a lot of humic acid and other organic materials that were collected in semi-closed karst depressions (initial bauxitic material sedimentary area) to form acidic water that favored Si removal (Fig. 13b).

(3) After long-term (hundreds to thousands years) Al enrichment and Si removal, the initial bauxitic material developed into a bauxitic material (higher gibbsite contents than initial bauxitic material) with a lower Si content. Subsequently, organic-rich sediment was deposited, which was precursor of "coal" of the "coal–bauxite–iron" structure at the top of the bauxite layer. The coal and/or carbonaceous rocks were then produce acidic and reducing groundwaters with organic materials that percolated downward, resulting in Al enrichment and the loss of Fe and Si of the underlying bauxitic materials (Fig. 13c) (Kalaitzidis et al., 2010). The removed Fe^{2+} translated to near the basal carbonates to precipitate the iron rocks (Fe_2O_3, FeS_2, $FeCO_3$, etc.) (Fig. 13d). Thus, the bauxitic material, which consists of gibbiste and clay minerals, experienced Fe and Si removal forming the initial bauxite or clay bauxite (mainly consist of boehmite and/or diaspore and clay minerals) after a certain geological period. It was verified by the ore textures, especially the diaspore lumps (Fig. 3b) of the Lindai deposit: the differences in texture between the kaolinite matrix and the diaspore lumps indicate that the precursor material of the diaspore was most likely gibbsite, because the gibbsite was the main aluminum mineral in laterite bauxite and diaspore and boehmite rarely occurred (Beneslavsky, 1974; Bárdossy, 1982; Meyer et al., 2002; Hanilçi, 2013). Besides, studies have shown a positive correlation between the thickness of the Lower Carboniferous Jiujialu Formation Al-bearing rock series in the central Guizhou and the lower segment "Qingzhen-type iron deposit" (Yang et al., 2011). The thicker the bauxite beds, the thicker the ferruginous rock layers, while the thinner the bauxite beds, the thinner the ferruginous rocks (Yang et al., 2011). This shows that bauxite beds were closely linked with the lower segment ferruginous rocks; with the increasing thickness of bauxite beds, more Fe^{2+} was translated down to lower segments by acidic and reducing groundwater, forming a thicker ferruginous rock layer.

(4) During the Late Trassic, the crust in the Guizhou area was uplifted and converted from sea to land (Guizhou Bureau of Geology and Mineral Resources, 1987). Tectonic movement uplifted the initial bauxite and clay bauxite to near the surface. The coal layers or carbonaceous shales continued to produce acidic and reducing groundwater to cause secondary alteration and enrichment of the initial bauxite and clay bauxite, ultimately forming the high-quality bauxite that is available for industrial exploitation. Supergene leaching process, however, may have improved the quality of bauxites, but could not convert argillaceous rock to bauxites.

Though abundant geological, mineralogical, and geochemical investigations of karstic bauxite deposits have been carried out to reveal the ore-forming process (Valeton, 1972; Bárdossy, 1982; D'Argenio and Mindszenty, 1995; Öztürk et al., 2002; Mameli et al., 2007; Karadağ et al., 2009; Liu et al., 2010; Zarasvandi et al., 2012; Wang et al., 2011a; Ling et al., 2013; Cai et al., 2015; Mongelli et al., 2015, 2016), the metallogenic model of karstic bauxite still remained controversy. Established models generally emphasize in situ alteration and production of residual material from the leaching of either the limestone or associated pyroclastic debris, which forms a blanket of bauxitic material on a karst surfaces (karst depressions or sinkholes). More specifically, the bauxite mainly formed in three stages: stage 1, the parent rocks were experienced strong chemical weathering and changed into the bauxitic materials (lateritic bauxite or Al-rich lateritic); stage 2, the bauxitic materials were upgraded changed into ores by in situ leaching and desilicification under conditions of well-developed karst drainage systems, since the bauxitic materials were transported a short distance to karst depressions and sinkholes; stage 3, tectonic movement uplifted the bauxite to near the surface experienced supergene leaching process, ultimately forming the high-quality bauxite (e.g., Bárdossy, 1982; D'Argenio and Mindszenty, 1995; Öztürk et al., 2002 Liu et al., 2010; Ling et al., 2013). Our model have some difference from those models: (1) this paper highlights the important of the hydrogeological conditions during bauxite mineralization and believed that acidic, reducing, and organic materials occurrences are essential hydrogeological conditions for high-quality karstic bauxite mineralization; (2) Si and Fe removal occur at different stages due to different chemical properties. Si was removal firstly under neutral and/or reducing inorganic acid condition, whereas Fe removal can occur only in acidic and reducing conditions with the presence of organic matter; (3) the "coal–bauxite–iron" structure greatly promoted the karstic bauxite formation.

7. Conclusions

(1) Existence of rutile within diaspore lumps that are inherited from laterization offers strong evidence that diaspore was transformed from gibbsite and karstic bauxite was transformed from laterite bauxite.

(2) The geochemical characteristics show that the underlying Shilengshui Formation dolomite is the precursor rock of the Lindai bauxite, and the weathered laterite is an intermediate product of the conversion process of parent rock to bauxite.

(3) Simulated weathering experiments show that Si is most likely to migrate in natural conditions, especially under reducing inorganic acid conditions; Fe migration is difficult with groundwater, Al enrichment and Fe removal are possible only under acidic and reducing conditions with organic matter.

(4) The "coal–bauxite–iron" structure occur in karstic bauxite were formed under specific conditions: during bauxite formation, coal beds or other rocks rich in organic material overlying the Al-bearing rock series produced acidic and reducing groundwater with organic materials, which were important for bauxite mineralization.

(5) The hydrogeological conditions are important for karst bauxite mineralization. Acidic, reducing, and organic materials presences are essential hydrogeological conditions for high-quality karstic bauxite formation during sedimenta tion–diagenesis processes.

(6) A theoretical model for the karstic bauxite mineralization in Central Guizhou Province in this paper is proposed (Fig. 13) and can explain the bauxite mineralization of the karstic bauxite deposits.

Acknowledgments

This study was funded by the Major Project of Chinese National Programs for Fundamental Research and Development (973 Program; Nos. 2014CB440906) and the National Natural Science Foundation of China (Nos. 41672086). The authors would like to thank researchers Liu Jiaren and Chen Wei for their help in the geological field investigation and researchers Zhang Zhengwei and Sheng Zhangqi for their guidance and assistance. We would also like to thank Dr. Sun Min for her assistance. We would like to acknowledge to prof. Franco Pirajno, M. Santosh, Hassan Zamanian, and another anonymous reviewer for their review and suggestions that improved our manuscript significantly.

References

Abedini, A., Calagari, A.A., 2013. Rare earth elements geochemistry of Sheikh-Marut laterite deposits, NW Mahabad, West-Azarbaijan province, Iran. Acta Geol. Sin.-Engl. 87, 176–185.
Al-Bassam, K.S., 2005. Mineralogy and geochemistry of the Hussainiyat karst bauxite and Zabira stratiform bauxite in northern Arabian Peninsula. Iraqi Bull. Geol. Min. 1, 15–44.
Anand, R.R., Gilkes, R.J., Roach, G.I.D., 1991. Geochemical and mineralogical characteristics of bauxites, Darling Range, Western Australia. Appl. Geochem. 6, 233–248.
Bárdossy, G., 1982. Karst Bauxites, Bauxite Deposits on Carbonate Rocks. Elsevier, Amsterdam, pp. 1–441.
Bárdossy, G., Aleva, G.J.J., 1990. Lateritic Bauxites. Elsevier, Amsterdam, p. 624.
Beneslavsky, S.I., 1974. Mineralogy of Bauxites. Nedra, Moscow, pp. 5–18 (in Russian).
Boni, M., Reddy, S.M., Mondillo, N., Balassone, G., Taylor, R., 2012. A distant magmatic source for Cretaceous karst bauxites of southern Apennines (Italy), revealed through SHRIMP zircon age dating. Terranova 24, 326–332.
Boni, M., Rollinson, G., Mondillo, N., Balassone, G., Santoro, L., 2013. Quantitative mineralogical characterization of karst bauxite deposits in the southern Apennines, Italy. Econ. Geol. 108, 813–833.
Boulangé, B., Bouzat, G., Pouliquen, M., 1996. Mineralogical and geochemical characteristics of two bauxitic profiles, Fria, Guinea Republic. Mineral. Deposita 31, 432–438.
Cai, S.H., Wang, Q.F., Liu, X.F., Feng, Y.W., Zhang, Y., 2015. Petrography and detrital zircon study of late Carboniferous sequences in the southwestern North China Craton: implication for the regional tectonic evolution and bauxite genesis. J. Asian Earth Sci. 98, 421–435.
Calagari, A.A., Abedini, A., 2007. Geochemical investigations on Permo-Triassic bauxite horizon at Kanisheeteh, east of Bukan, West-Azarbaidjan, Iran. J. Geochem. Explor. 94, 1–18.
Chen, L., 1991. Experimental research of elemental differentiations in the forming process of bauxite. Acta Sediment. Sin. 9, 87–95 (in Chinese with English abstract).
Chen, L., 1996. Experimental study of action of humic acids in the processes of bauxite mineralization. Acta Sediment. Sin. 14, 117–123 (in Chinese with English abstract).
Clarke, O.M., 1966. The formation of bauxite on karst topography in Eufaula district, Labama, and Jamaica, West Indies. Econ. Geol. 61, 903–916.
Combes, P.J., 1969. Observations et interprétations nouvelles sur les bauxites du nord-est de l'Espagne (stratigraphie, paléogéographie, génèse). Annales Instituti Geologici Publici Hungarici. v. 54, pp. 265–280.
Crnicki, J., Jurkovic, I., 1990. Rare earth elements in Triassic bauxites of Croatia Yugoslavia. Travaux 19, 239–248.
D'Argenio, B., Mindszenty, A., 1995. Bauxites and related paleokarst: tectonic and climatic event markers at regional unconformities. Eclogae Geol. Helv. 88, 453–499.
Demina, V.N., 1977. Bauxites of the Middle and South Timan Nauka, Moscow, pp. 1–136 (in Russian).
Deng, J., Wang, Q.F., Yang, S.J., Liu, X.F., Zhang, Q.Z., Yang, L.Q., Yang, Y.H., 2010. Genetic relationship between the Emeishan plume and the bauxite deposits in western Guangxi, China: constraints from U-Pb and Lu–Hf isotopes of the detrital zircons in bauxite ores. J. Asian Earth Sci. 37, 412–424.
Du, Y., Tong, J., 1998. Introduction to paleontology and historical geology. China University of Geosciences Press, pp. 1–202 (in Chinese).
Esmaeily, D., Rahimpour-Bonab, H., Esna-Ashari, A., Kananian, A., 2010. Petrography and geochemistry of the Jajarm Karst bauxite ore deposit, NE Iran: implications for source rock material and ore genesis. Turk. J. Earth Sci. 19, 267–284.
Franzini, M., Leoni, L., Saitta, M., 1972. A simple method to evaluate the matrix effects in X-ray fluorescence analysis. X-Ray Spectrom. 1, 151–154.
Gao, D., Sheng, Z., Shi, S., Chen, L., 1992. Studies on the Bauxite Deposit in Central Guizhou, China. Guizhou Science & Technology Publishing House, Guiyang, pp. 11–20 (in Chinese).
Grubb, P.L.C., 1970. Mineralogy, geochemistry, and genesis of the bauxite deposits on the Gove and Mitchell Plateaux, Northern Australia. Mineral. Deposita 5, 248–272.
Grubb, P.L.C., 1979. Genesis of bauxite deposits in the lower Amazon Basin and Guianas Coastal Plain. Econ. Geol. 74, 735–750.
Gu, J., Huang, Z.L., Fan, H.P., Jin, Z.G., Yan, Z.F., Zhang, J.W., 2013a. Mineralogy, geochemistry, and genesis of lateritic bauxite deposits in the Wuchuan–Zheng'an–Daozhen area, northern Guizhou Province, China. J. Geochem. Explor. 130, 44–59.
Gu, J., Huang, Z.L., Fan, H.P., Ye, L., Jin, Z.G., 2013b. Provenance of lateritic bauxite deposits in the Wuchuan–Zheng'an–Daozhen area, northern Guizhou Province, China: LA-ICP-MS and SIMS U-Pb dating of detrital zircons. J. Asian Earth Sci. 70–71, 265–282.
Guizhou Bureau of Geology and Mineral Resources, 1987. Regional geology of Guizhou Province. Geological Publishing House, Beijing, pp. 555–557 (in Chinese).
Han, N., Thompson, M.L., 1999. Copper-binding ability of dissolved organic matter derived from anaerobically digested biosolids. J. Environ. Qual. 28, 939–944.
Hanilçi, N., 2013. Geological and geochemical evolution of the Bolkardağı bauxite deposits, Karaman, Turkey: transformation from shale to bauxite. J. Geochem. Explor. 133, 118–137.
Horbe, A.M.C., Anand, R.R., 2011. Bauxite on igneous rocks from Amazonia and southwestern of Australia: implication for weathering process. J. Geochem. Explor. 111, 1–12.
Ji, H.B., Wang, S.J., Ouyang, Z.Y., Zhang, S., Sun, C.X., Liu, X.M., Zhou, D.Q., 2004. Geochemistry of red residua underlying dolomites in karst terrains of Yunnan-Guizhou Plateau I. The formation of the Pingba profile. Chem. Geol. 203, 1–27.
Joachimski, M.M., Von Bitter, P.H., Buggisch, W., 2006. Constraints on Pennsylvanian glacioeustatic sea-level changes using oxygen isotopes of conodont apatite. Geology 34, 277–280.
Kalaitzidis, S., Siavalas, G., Skarpelis, N., Araujo, C.V., Christanis, K., 2010. Late Cretaceous coal overlying karstic bauxite deposits in the Parnassus-Ghiona Unit, central Greece: coal characteristics and depositional environment. Int. J. Coal Geol. 81, 211–226.
Karadağ, M.M., Küpeli, S., Arýk, F., Ayhan, A., Zedef, V., Döyen, A., 2009. Rare earth element (REE) geochemistry and genetic implications of the Mortas bauxite deposit (Seydis, ehir/Konya–southern Turkey). Chem. Erde-Geochem. 69, 143–159.
Komlóssy, G.Y., 1970. The Iszkas zentgyörgy bauxite (SE Bakony Mts., Hungary). Problems of genesis and mineral formation. Ann. Inst. Geol. Public. Hung. 54, 347–358.
Kuiters, A.T., Mulder, W., 1992. Gel permeation chromatography and Cu-binding of water-soluble organic substances from litter and humus layers of forest soils. Geoderma 52, 1–15.
Laskou, M., Economou-Eliopoulos, M., 2007. The role of microorganisms on the mineralogical and geochemical characteristics of the Parnassos-Ghiona bauxite deposits, Greece. J. Geochem. Explor. 93, 67–77.
Laskou, M., Economou-Eliopoulos, M., 2013. Bio-mineralization and potential biogeochemical processes in bauxite deposits: genetic and ore quality significance. Mineral. Petrol. 107, 471–486.
Laznicka, P., 2006. Giant Metallic Deposits: Future Sources of Industrial Metals. Springer, Heidelberg, p. 719.
Leanard, J., 1982. Bauxite. Society of Mining Engineers of America Institute, New York.
Li, Z., Din, J., Xu, J., Liao, C., Yin, F., Lv, T., Cheng, L., Li, J., 2013. Discovery of the REE minerals in the Wulong-Nanchuan bauxite deposits, Chongqing, China: insights on conditions of formation and processes. J. Geochem. Explor. 133, 88–102.
Ling, K., Zhu, X., Wang, Z., Han, T., Tang, H., Chen, W., 2013. Metallogenic model of bauxite in Central Guizhou Province: an example of Lindai deposit. Acta Geol. Sin.-Engl. 87, 1630–1642.
Ling, K.Y., Zhu, X.Q., Tang, H.S., Wang, Z.G., Yan, H.W., Han, T., Chen, W.Y., 2015. Mineralogical characteristics of the karstic bauxite deposits in the Xiuwen ore belt, Central Guizhou Province, Southwest China. Ore Geol. Rev. 65, 84–96.
Liu, P., Liao, Y., 2013. The zonation and genetic mechanism of Zunyi high-and low ferrous bauxite. Geol. China 40, 949–966 (in Chinese with English abstract).
Liu, X., Wang, Q., Chen, Y., Qin, D., 1990. Bauxite minerogenic geological characteristic and minerogenic law in Northern Guizhou, China. Guizhou People's Publishing House, Guiyang, pp. 131–136 (in Chinese).
Liu, X.F., Wang, Q.F., Deng, J., Zhang, Q.Z., Sun, S.L., Meng, J.Y., 2010. Mineralogical and geochemical investigations of the Dajia Salento-type bauxite deposits, Western Guangxi, China. J. Geochem. Explor. 105, 137–152.
Liu, X.F., Wang, Q.F., Zhang, Q.Z., Feng, Y.W., Cai, S.H., 2012. Mineralogical characteristics of the superlarge Quaternary bauxite deposits in Jingxi and Debao counties, western Guangxi, China. J. Asian Earth Sci. 52, 53–62.
Ma, J.L., Wei, G.J., Xu, Y.G., Long, W.G., Sun, W.D., 2007. Mobilization and redistribution of major and trace elements during extreme weathering of basalt in Hainan island, south China. Geochim. Cosmochim. Acta 71, 3223–3237.
MacLean, W.H., 1990. Mass change calculations in altered rock series. Mineral. Deposita 25, 44–49.

MacLean, W.H., Bonavia, F.F., Sanna, G., 1997. Argillite debris converted to bauxite during karst weathering: evidence from immobile element geochemistry at the Olmedo deposit, Sardinia. Mineral. Deposita 32, 607–616.
Maksimovic, Z., Panto, G., 1991. Contribution to the geochemistry of the rare earth elements in the karst–bauxite deposits of Yugoslavia and Greece. Geoderma 51, 93–109.
Mameli, P., Mongelli, G., Oggiano, G., Dinelli, E., 2007. Geological, geochemical and mineralogical features of some bauxite deposits from Nurra (western Sardinia, Italy): insights on conditions of formation and parental affinity. Int. J. Earth Sci. 96, 887–902.
Meyer, F.M., Happel, U., Hausberg, J., Wiechowski, A., 2002. The geometry and anatomy of the Los Pijiguaos bauxite deposit, Venezuela. Ore Geol. Rev. 20, 27–54.
Mongelli, G., 1997. Ce-anomalies in the textural components of Upper Cretaceous karst bauxites from the Apulian Carbon ate Platform (southern Italy). Chem. Geol. 140, 69–79.
Mongelli, G., Boni, M., Buccione, R., Sinisi, R., 2014. Geochemistry of the Apulian karst bauxites (southern Italy): chemical fractionation and parental affinities. Ore Geol. Rev. 63, 9–21.
Mongelli, G., Buccione, R., Sinisi, R., 2015. Genesis of autochthonous and allochthonous Apulian karst bauxites (Southern Italy): climate constraints. Sediment. Geol. 325, 168–176.
Mongelli, G., Buccione, R., Gueguen, E., Langone, A., Sinisi, R., 2016. Geochemistry of the apulian allochthonous karst bauxite, Southern Italy: distribution of critical elements and constraints on Late Cretaceous Peri-Tethyan palaeogeography. Ore Geol. Rev. 77, 246–259.
Mordberg, L.E., Stanley, C.J., Germann, K., 2000. Rare earth element anomalies in crandallite group minerals from the Schugorsk bauxite deposit, Timan, Russia. Eur. J. Mineral. 12, 1229–1243.
Nesbitt, H.W., Yong, G.M., 1982. Early Proterozoic climates and plate motions inferred from major element chemistry of lutites. Nature 299, 715–717.
Özlü, N., 1983. Trace element contents of karst bauxites and their parent rocks in the Mediterranean belt. Mineral. Deposita 18, 469–476.
Öztürk, H., Hein, J.R., Hanilçi, N., 2002. Genesis of the Dogankuzu and Mortas bauxite deposits, Taurides, Turkey: separation of Al, Fe, and Mn and implications for Passive Margin Metallogeny. Econ. Geol. 97, 1063–1077.
Patterson, S.H., 1967. Bauxite Reserves and Potential Aluminum Resources of the World. U.S. Geological Survey Bulletin, p. 1228.
Potts, P.J., Thompson, M., Kane, J.S., Petrov, L.L., 2000. GEOPT7–an international proficiency test for analytical geochemistry laboratories. Report on Round. Geostand. Geoanal. Res. 7, 35.
Potts, P.J., Thompson, M., Webb, P.C., Watson, J.S., 2001. GEOPT9–an international proficiency test for analytical geochemistry laboratories. Report on Round. Geostand. Geoanal. Res. 9, 36.
Qi, L., Hu, J., Gregoire, D.C., 2000. Determination of trace elements in granites by inductively coupled plasma mass spectrometry. Talanta 51, 507–513.
Radusinović, S., Jelenković, R., Pačevski, A., Simić, V., Božović, D., Holclajtner-Antunović, I., Životić, D., 2017. Content and mode of occurrences of rare earth elements in the Zagrad karstic bauxite deposit (Nikšić area, Montenegro). Ore Geol. Rev. 80, 406–428.
Smith, P., 2009. The processing of high silica bauxites—review of existing and potential processes. Hydrometallurgy 98, 162–196.
Sun, S.S., McDonough, W.F., 1989. Chemical and isotopic systematics of oceanic basalts: implications for mantle composition and processes. Geol. Soc. Lond. Spec. Publ. 42, 313–345.
Temur, S., Kansun, G., 2006. Geology and petrography of the Masatdagi diasporic bauxites, Alanya, Antalya, Turkey. J. Asian Earth Sci. 27, 512–522.
Thompson, M., Potts, P.J., Kane, J.S., Wilson, S., 1999. GEOPT5–an international proficiency test for analytical geochemistry laboratories. Report on Round. Geostand. Geoanal. Res. 5, 23.
USGS, 2009. Mineral Commodity Summaries: Bauxite and alumina. United States Government Printing Office, Washington, pp. 1–8.
Valeton, I., 1972. Bauxite, Development in soil science V.1. Elsevier Publishing Company, London, pp. 1–142.
Valeton, I., Biermann, M., Reche, R., Rosenberg, F., 1987. Genesis of nickel laterites and bauxites in Greece during th e Jurassic and Cretaceous, and their relation to ultrabasic parent rocks. Ore Geol. Rev. 2, 359–404.
Wang, Q.F., Deng, J., Liu, X.F., Zhang, Q.Z., Sun, S.L., Jiang, C.Z., Zhou, F., 2010. Discovery of the REE minerals and its geological significance in the Quyang bauxite deposit, West Guangxi, China. J. Asian Earth Sci. 39, 701–712.
Wang, Q.F., Deng, J., Zhang, Q.Z., Liu, H., Liu, X.F., Wan, L., Li, N., Wang, Y.R., Jiang, C. Z., Feng, Y.W., 2011a. Orebody vertical structure and implications for ore-forming processes in the Xinxu bauxite deposit, Western Guangxi, China. Ore Geol. Rev. 39, 230–244.
Wang, Y., Li, Z., Zhai, Z., Li, R., Li, X., 2011b. Benxi Formation bauxite mineralization condition and rule in Shanxi Province. Northwest Geol. 44, 82–88 (in Chinese with English abstract).
Wang, Q.F., Liu, X.F., Yan, C.H., Cai, S.H., Li, Z.M., Wang, Y.R., Zhao, J.M., Li, G.J., 2012. Mineralogical and geochemical studies of boron-rich bauxite ore deposits in the Songqi region, SW Henan, China. Ore Geol. Rev. 48, 258–270.
Wang, Q., Deng, J., Liu, X., Zhao, R., Cai, S., 2016. Provenance of Late Carboniferous bauxite deposits in the North China Craton: new constraints on marginal arc construction and accretion processes. Gondwana Res. 38, 86–98.
Weng, S., Lei, Z., Chen, H., Zhao, S., Ran, Y., Wang, X., Ge, C., 2013. Relationship between basal paleogeomorphology and bauxite ore quality in the Wuchuan–Zheng'an–Daozhen area: an example from the dazhuyuan bauxite ore deposit. Geol. Explor. 49, 195–204 (in Chinese with English abstract).
White, A.F., Blum, A.E., Schulz, M.S., Bullen, T.D., Harden, J.W., Peterson, M.L., 1996. Chemical weathering rates of a soil chronosequence on granitic alluvium: I. Quantification of mineralogical and surface area changes and calculation of primary silicate reaction rates. Geochim. Cosmochim. Acta 60, 2533–2550.
Wu, P., Tang, C., Liu, C., Zhu, L., Pei, T., Feng, L., 2009. Geochemical distribution and removal of As, Fe, Mn and Al in a surface water system affected by acid mine drainage at a coalfield in Southwestern China. Environ. Geol. 57, 1457–1467.
Yang, R., Yuan, S., Wei, H., Chen, J., Cheng, M., 2011. Sediment geochemical character of carboniferous "Qingzhen-type Fe deposit" in central Guizhou area. Geol. Rev. 57, 24–35 (in Chinese with English abstract).
Ye, L., Cheng, Z., Pan, Z., 2007. The REE geochemical characteristics of the Xiaoshanba bauxite deposit, Guizhou. Bull. Mineral. Petrol. Geochem. 26, 228–233 (in Chinese with English abstract).
Yu, W., Ruihu, W., Qilian, Z., Yuansheng, D., Yue, C., Yuping, L., 2014. Mineralogical and geochemical evolution of the Fusui bauxite deposit in Guangxi, South China: from the original Permian orebody to a Quarternary Salento-type deposit. J. Geochem. Explor. 146, 75–88.
Zamanian, H., Ahmadnejad, F., Zarasvandi, A., 2016. Mineralogical and geochemical investigations of the Mombi bauxite deposit, Zagros Mountains. Iran. Chem. Erde-Geochem. 76, 13–37.
Zarasvandi, A., Zamanian, H., Hejazi, F., 2010. Immobile elements and mass changes geochemistry at Sar-Faryab bauxite deposit, Zagros Mountains. Iran. J. Geochem. Explor. 107, 77–85.
Zarasvandi, A., Carranza, E.J.M., Ellahi, S.S., 2012. Geological, geochemical, and mineralogical characteristics of the Mandan and Deh-now bauxite deposits, Zagros Fold Belt, Iran. Ore Geol. Rev. 48, 125–138.
Zhang, Z., Zhou, L., Li, Y., Wu, C., Zheng, C., 2013. The "coal-bauxite-iron" structure in the ore-bearing rock series as a prospecting indicator for southeastern Guizhou bauxite mines. Ore Geol. Rev. 53, 145–158.